The transcriptome of regenerating zebrafish scales identifies genes involved in human bone disease

Dylan J.M. Bergen[1,2*], Qiao Tong[1], Ankit Shukla[3], Elis Newman[1], Jan Zethof[4], Mischa Lundberg[3,5], Rebecca Ryan[1], Scott E. Youlten[6,7], Eleftheria Zeggini[8,9], Peter I. Croucher[6,7,10], Gert Flik[4], Rebecca J. Richardson[1], John P. Kemp[3,11,$], Chrissy L. Hammond[1,$] and Juriaan R. Metz[4,$*]

[$]Contributed equally to this work

[*]Corresponding authors

dylan.bergen@bristol.ac.uk

j.metz@fnwi.ru.nl

Affiliation:

1 School of Physiology, Pharmacology, and Neuroscience, Faculty of Life Sciences, University of Bristol, Bristol, United Kingdom

2 Musculoskeletal Research Unit, Translational Health Sciences, Bristol Medical School, Faculty of Health Sciences, University of Bristol, Bristol, United Kingdom

3 The University of Queensland Diamantina Institute, University of Queensland, Woolloongabba, Queensland, Australia

4 Department of Animal Ecology and Physiology, Institute for Water and Wetland Research, Faculty of Science, Radboud University Nijmegen, Netherlands

5 Transformational Bioinformatics, Commonwealth Scientific and Industrial Research Organisation, Sydney, New South Wales, Australia

6 Bone Biology, Garvan Institute of Medical Research, Sydney, New South Wales, Australia

7 St Vincent's Clinical School, Faculty of Medicine, UNSW Australia, Sydney New South Wales, Australia

8 Institute of Translational Genomics, Helmholtz Zentrum Munchen, Neuherberg, Germany

9 TUM School of Medicine, Technical University of Munich and Klinikum Rechts der Isar, Munich, Germany

10 School of Biotechnology and Biomolecular Sciences, UNSW Australia, Sydney, New South Wales, Australia

11 Medical Research Council Integrative Epidemiology Unit, Population Health Sciences, Bristol Medical School, University of Bristol, Bristol, United Kingdom

Key words: bone, collagen, osteoblast, musculoskeletal disease, zebrafish, scales

Abstract

Zebrafish scales are mineralised plates that can regenerate involving *de novo* bone formation. This presents an opportunity to uncover genes and pathways relevant to human musculoskeletal disease relevant to impaired bone formation. To investigate this hypothesis, we defined transcriptomic profiles of ontogenetic and regenerating scales, and identified 604 differentially expressed genes (DEGs) that were enriched for extracellular matrix, ossification, and cell adhesion pathways. Next, we showed that human orthologues of DEGs were 2.8 times more likely to cause human monogenic skeletal diseases ($P<8\times10^{-11}$), and they showed enrichment for human orthologues associated with polygenetic disease traits including stature, bone density and osteoarthritis ($P<0.005$). Finally, zebrafish mutants of two human orthologues that were robustly associated with height and osteoarthritis (*COL11A2*) or bone density only (*SPP1*) developed skeletal abnormalities consistent with our genetic association studies. *Col11a2*$^{Y228X/Y228X}$ mutants showed endoskeletal features consistent with abnormal growth and osteoarthritis, whereas *spp1*$^{P160X/P160X}$ mutants had elevated bone density ($P<0.05$). In summary, we show that transcriptomic studies of regenerating zebrafish scales have potential to identify new genes and pathways relevant to human skeletal disease.

Introduction

The zebrafish skeleton, similar to higher vertebrates, provides structure, organ protection, endocrine and locomotive function. During development, bone is formed by two evolutionarily conserved processes via either endochondral or intramembranous (dermal) ossification. Endochondral bone formation occurs though progressive remodelling of a cartilage template into bone, while dermal or intramembranous bone is formed directly by mesenchymal condensation of osteoblasts. Due to mechanical loading induced microfractures, bone is a dynamic tissue that undergoes constant remodelling of the calcified extracellular matrix (ECM) via a tight coupling between the functional activity of the bone-building osteoblasts and bone-degrading osteoclasts, allowing a regenerative capacity of bone throughout life (Kenkre & Bassett, 2018). In common age-related conditions such as osteoporosis, this balance is dysregulated such that catabolism exceeds anabolism, making bone more fragile and susceptible to fracture. Current pharmacotherapies for osteoporosis are limited, with most targeting the catabolic activity of osteoclasts rather than on bone anabolism. However, human genetic studies of rare bone diseases have shed light on potential bone anabolic pathways leading to development of novel therapeutics (Pathak, Bravenboer et al., 2020). For example, linkage studies have identified the WNT pathway inhibitor Sclerostin (SOST) that leads to Sclerosteosis causing high bone mass (HBM) in humans and mice when mutated (Balemans, Ebeling et al., 2001, Li, Ominsky et al., 2008). The subsequent development of a humanised monoclonal antibody (Romozumab) against SOST now offers an osteo-anabolic therapeutic that reduces fracture risk for osteoporosis patients (Cosman, Crittenden et al., 2016). This demonstrates how understanding the genetic control of bone growth and osteoblast differentiation processes allow identification of novel therapeutic targets.

One potential route to identifying new pathways and targets is through the study of organisms and tissues capable of rapid regrowth of skeletal tissues, during which bone anabolism exceeds bone catabolism. While skeletal regenerative capacity in mammals is limited to bone remodelling and fracture healing, a number of other vertebrates species such as zebrafish are able to undergo epimorphic regeneration of many organs throughout life, including the bony structures of the fins and scales (Zhao, Qin et al., 2016). Zebrafish are increasingly used as a model for musculoskeletal (MSK) research, due to their genetic tractability, availability of transgenic reporter lines and the dynamic imaging opportunities, they offer as well as the similarities of their skeletal physiology to humans and other higher vertebrates (Lleras-Forero, Winkler et al., 2020). Zebrafish fin regeneration has been extensively studied and has revealed many of the mechanisms that underpin blastema

formation and skeletal dedifferentiation and re-differentiation during tissue regrowth (Sehring & Weidinger, 2020).

Most teleost fishes have scales which function as a protective armour and a calcium reservoir (Sire, Donoghue et al., 2009, Yasuo, 1980).The zebrafish elasmoid scales, that also undergo complete epimorphic regeneration within days to weeks, have recently gained attention in studies aiming at deeper understanding of mechanisms of bone growth, regeneration, and repair. In common with intramembranous flat bones, the elasmoid scales are formed and mineralised directly by *de novo* differentiated osteoblasts (Pasqualetti, Banfi et al., 2012, Sire, Allizard et al., 1997). Scales are exoskeletal elements that have been strongly reduced or completely lost in terrestrial animals during evolution but have been retained in bony fish. Long regarded to be odontogenic in origin, relatively recent studies have provided new insights into the classification of skeletal structures and evolutionary and developmental origins of exoskeletal teleost scales (Dhouailly, Godefroit et al., 2019, Shimada, Kawanishi et al., 2013). Following removal of the ontogenetic scale from the dermal socket initiating a wound healing inflammation phase, regeneration is initiated and a small mineralised scale plate can be observed as early as two days post-harvest (dph) (Bereiter-Hahn & Zylberberg, 1993, Richardson, Slanchev et al., 2013, Sire & Akimenko, 2004). Regenerating scales have a high density of osteoblasts at the posterior edge of the plate forming the leading growth plane whose dynamics can be tracked *in toto* (Cox, De Simone et al., 2018). These osteoblasts form a (hyposquamal) monolayer and deposit hydroxyapatite into a type I collagen rich matrix that can be resorbed by osteoclasts (de Vrieze, Sharif et al., 2011, Guellec & Zylberberg, 1998). The collagen matrix of scales is organised in a plywood manner resembling lamellar bone in humans (Bergen, Kague et al., 2019, Bigi, Burghammer et al., 2001, Giraud-Guille, 1988). Similar to human bones, scale bone turnover responds to exposure of prednisolone, alendronate, chronic hyperglycaemia, and fatty acids (e.g. OMEGA-6) highlighting evolutionarily conserved mechanisms of bone metabolism (Carnovali, Luzi et al., 2016, Carnovali, Ottria et al., 2016, de Vrieze, van Kessel et al., 2014, Pasqualetti, Congiu et al., 2015). Moreover, ontogenetic scales show a fracture healing response with recruitment of *trapc* expressing cells to the fracture site (Kobayashi-Sun, Yamamori et al., 2020). The possibility to *ex vivo* culture fish scales as small transparent bone units, in which vital intercellular interactions (between osteoblasts and osteoclasts), as well as cell-matrix interactions remain intact, has triggered their use in screenings for osteogenic compounds (de Vrieze et al., 2011, de Vrieze, Zethof et al., 2015). Hence, these features therefore warrant a deeper analysis of genes, pathways in the scale and a comparison with genes associated with human MSK disease.

113 As regeneration leads to rapid bone regrowth we hypothesised that (i) osteoanabolic genes can be
114 identified by contrasting the transcriptomic profiles of ontogenetic and regenerating zebrafish
115 scales, and (ii) that these identified “bone formation” genes were likely to be enriched for human
116 orthologues that influence bone growth, mineralisation and susceptibility to MSK disease. To test
117 our hypotheses, we identified differentially expressed genes (DEGs) that distinguished regenerating
118 scales from ontogenetic scales, identified biological pathways that DEGs were involved in, and
119 investigated whether DEGs were associated with human monogenic disease, and polygenetic
120 disease traits: height, bone mineral density and osteoarthritis susceptability. Lastly, we performed
121 functional studies of two DEGs that were robustly associated with one or more human MSK disease
122 traits and observed abnormal endoskeletal phenotypes consistent with the human genetic
123 association analyses.

124 *Results*

125 **Defininig the transcriptome of ontogentic and regenerating scales by RNA-sequencing**

126 We first confirmed that,regenerating scales show an increase in the number of *sp7* positive
127 osteoblasts compared to original scales formed during development (ontogenetic) as previously
128 reported (Cox et al., 2018, de Vrieze et al., 2014) (**figure 1A**). Alkaline phosphatase (ALP) staining
129 showed that regenerating scales contained more ALP activity (**figure 1B**). To identify the biological
130 pathways underpinning the regeneration process, we preformed RNA-sequencing (RNA-seq) on
131 ontogenetic (original) and regenerating scales 9 days into their regeneration (**figure 1C**).

132 A total of 13,170 protein coding genes were consistently expressed (i.e. 51.4% of total protein
133 coding genome) in both ontogentic and regenerating scales (**data file S1**). Principal component
134 analysis (PCA) of the two groups of all genes expressed showed that ontogenetic and regenerating
135 scale groups cluster together (**figure S1A**) and that there was a a high level of correlation (Pearson's
136 correlation of 97.1%, **figure S1B**), confirming similar expression patterns within the PCA groups.
137 Setting the arbitrary threshold at 1.25 $\log_2$ fold change and a false discovery rate (FDR) of <0.05
138 showed that 604 protein coding genes had substantial differences in gene expression (**data file S2**).
139 We observed a skew towards upregulation of genes (*n = 514* compared to *n = 90* downregulated);
140 consistent with regenerating tissues such as the caudal fin (Padhi, Joly et al., 2004, Schmidt,
141 Geurtzen et al., 2019) (**figure 1D**). The osteoblast transcription factor *sp7(osxterix)* was substantially
142 upregulated (2.39 $\log_2$ fold change) in regenerating scales (**figure 1D**), but 128 genes showed a larger
143 up regulation than *sp7*. Among the top DEGs, we noticed a high number of collagen and cell
144 adhesion related genes (**table 1**).Two genes were highly downregulated and a homology search
145 revealed that both genes encoded different proteins [i.e. ENSDARG00000068621 (*si:ch211-181d7.3*)
146 and ENSDARG00000088274 (*si:ch211-181d7.1*)] that were unique to fish(**figure S2**). Both genes have
147 NOD-like receptor (NLR) domains that possess NACHT (NTPase) and leucine-rich repeat (LRR) protein
148 domains important for innate immune system antigen interactions (Wu, Chen et al., 2018).

149 Osteoblast factors such as *sp7, entpd5a/b, postnb, smpd3, phospho1, plod1a, plod2,* and *plod3* were
150 upregulated in 9 dph scales, as were genes related to ECM growth, collagens (predominantly fibrillar
151 collagens) and collagen remodelling including *bmp1a*, *mmp9*, *spp1*, *ostn*, *col1a1a/b*, *col1a2*, *col5a1,*
152 *col5a2a/b, col10a1a/b*, *bgna/b*, *col11a1a/b* and *col11a2* (Ricard-Blum, 2011). We also observed
153 elevated expression of genes normally associated with endochondral ossification: *col11a1a/b* and
154 *col11a2, ihha, ptch2, dlx5a,* and *mef2cb*, suggesting that some genes are common to both modes of
155 ossification (Long & Ornitz, 2013). While osteoclast and monocyte related factors (e.g. *tnfrsf11a*
156 (*RANK*), chloride channel *clc7n7, cathepsin-K* (*ctsk*), and *acp5a/b (trapc*)) were expressed in both

157 ontogenetic and regenerating scales, differential expression was not observed (**data file S1**). To
158 validate the RNA-seq dataset, quantitative real-time PCR (qRT-PCR) was performed on osteoblast
159 and osteoclast markers and showed concordant data between RNA-seq and qRT-PCR assays of all
160 selected amplicons (**figure 2A**). These results indicate osteoblast activity is elevated to a greater
161 degree than osteoclast activity. To visualise newly formed bone, *in vivo* calcein green staining was
162 performed (**figure 2B**). The calcein green signal was stronger in regenerating scales, and
163 predominantly seen in the posterior regions of the scale, consistent with elevated expression of
164 bone anabolic factors such as *sp7* and *entpd5a* (**figure 2A** and **2B**).

165 **The collagen processing pathway is highly enriched and upregulated during scale regeneration**

166 To identify biological pathways overrepresented among DEGs, we performed gene ontology (GO)
167 enrichment analysis. Several, bone specific GO terms were significantly overrepresented among
168 DEGS, such as 'regulation of bone biomineralization' (GO:0110149; 10.9-fold, FDR=0.018),
169 'ossification' (GO:0001503; 6.0-fold, FDR=0.0019), and 'skeletal system development' (GO:0001501;
170 3.6-fold, FDR=5.3×10^{-6}). Collagen related terms were also significantly enriched (>7.1 fold,
171 FDR=8.7×10^{-6}) (**figure 2C, data file S3**), including 'collagen trimer', 'collagen-containing extracellular
172 matrix' and 'fibrillar collagen trimer' GO terms (**figure 2D**). Additional bone matrix associated
173 processes such as 'calcium-ion binding', 'glycosaminoglycan binding' and. 'matrix metalloprotease
174 (MMP) activity' were identified (**figure S3 and S4**). Further, the 'integrin signalling pathway' (P00034;
175 3.5-fold, FDR=0.016) was the only enriched signalling pathway, which is known to bind collagen
176 during cell adhesion related processes (Zeltz & Gullberg, 2016) (**data file S4**). Together, this indicated
177 DEGs were enriched for biological pathways involved in bone formation and collagen-matrix
178 synthesis, consistent with increased osteoblast activity.

179 We next visualised protein-protein interactions (PPI) within this set using STRING Network analysis.
180 This broadly confirmed GO findings and showed that the DEGs PPI network has 6.6-fold higher
181 number of nodes (connections) compared to the whole reactome ($P<1.0 \times 10^{-16}$). There were ten
182 clusters with distinct functions that were significantly enriched that were highly associated with
183 collagen-rich ECM and cell adhesion (**figure 3**). Additional terms not identified by GO included
184 'regulation of insulin-like growth factor (IGF) signalling' and 'signalling by hedgehog' (HH) (**figure 3**).
185 Note that STRING added 10 'high-scoring' interactors to the network that were not DEGs (**figure**
186 **S5A**). There were four clusters unlinked to the main network, related to cytoskeletal structure or cell
187 motility such as actin-myosin (cluster 1 and 4), cell motility proteins that regulate leading edge
188 cytoskeletal modelling (cluster 2), and enzyme function (cluster 3) (**figure 3** and **table S1**). Allowing
189 less stringent interaction evidence scores (≥ 0.4) showed that *sp7* and *secreted phospho protein 1*

190 (*spp1*, encoding Osteopontin (Opn)) factors have connections with both the collagen and bone factor
191 clusters, the latter showing many connections to adjacent osteogenic clusters that for example
192 contain *phospo1* and *ostn* (**figure S5B**). These findings were verified with PANTHER 'Reactome
193 pathways' analysis (**data file S5**). These GO and PPI analyses showed that the RNA-seq dataset is
194 specific for an osteogenic collagen rich regenerating tissue.

195 We next verified RNA expression of *col1a2,* osteoblast deposited collagen *col10a1a,* the collagen
196 nucleation factor proteoglycan *bgna,* and hedgehog signalling ligand *ihha* that represent some of
197 these clusters identified above. The expression of the gap junction gene *cx43* was also assessed as it
198 regulates fin regeneration growth, and within our PPI network it was connected to the IGF cluster
199 known to modulate bone growth (Bhattacharya, Hyland et al., 2020). These amplicons were
200 assessed in regenerating scales from an independent experiment and all showed similar trends
201 between RNA-seq and qRT-PCR, validating these findings (**figure 4A**). Note, a subset of genes
202 showed similar profiles between the RNA-seq and independent experiments (**figure S6**). Ontogenetic
203 scales showed weak *col1a1a* expression, predominantly located in the epidermis adjacent to *sp7*
204 positive cells at the posterior edge of the scale (**figure 4B**). In regenerating scales, *col1a1a* promoter
205 activity was elevated along with expanded *sp7* expression covering most of the bony unit. We
206 observed elevated activity at newly forming circuli associated with thickening of the calcified ECM
207 (**figure 2B** and **figure 4B**). We performed the same procedure in *col10a1a:Citrine* and
208 *col2a1a:mChrerry* double transgenic zebrafish where the *col2a1a* reporter functions as a negative
209 control as it was not a DEG. This showed that ontogenetic reporter expression of both transgenes
210 was absent. At 9 dph, *col10a1a* reporter expression was observed at the posterior edge of the scale
211 and interestingly also at the newly developing circuli (thicker ECM) located at the anterior region of
212 the scale (**figure 4C**). A mCherry signal was not detected in ontogenetic or regenerating scales. These
213 findings confirm that the RNA-seq dataset of regenerating scales contains gene networks with osteo-
214 active factors that actively assemble (nucleate) a calcified collagen-rich matrix.

215 **Differentially expressed genes are enriched for human orthologues that cause monogenic skeletal**
216 **disease, and that associate with polygenic musculoskeletal traits and disease**

217 Next, we used a Fisher's Exact test of independence, in conjunction with the ISDS Nosology and
218 Classification of Skeletal Disorders database (Mortier, Cohn et al., 2019) to show that human
219 orthologues of zebrafish DEGs were 2.8 times more likely to cause monogenic skeletal dysplasia in
220 humans than expected by chance ($P=8\times10^{-11}$) (**figure 5A**). Specifically, human orthologues of 47 DEGs
221 resulted in one or more primary bone dysplasia in humans when mutated (**data file S6**). Subgroup
222 analysis revealed further evidence of of enrichment for genes that cause: 'Osteogenesis Imperfecta

223 and decreased bone density' (8-fold enrichment, $P=7.9\times10^{-10}$), 'abnormal bone mineralisation' (7-fold,
224 $P=1.6\times10^{-3}$), 'collagen type 11' (18-fold, $P=3.1\times10^{-3}$), 'metaphyseal dysplasia' (6.7-fold, $P=7.9\times10^{-3}$),
225 and several others (**figure 5B & data file S6**).
226
227 MAGMA competitive gene set analysis was used to investigate the relationship between genetic
228 variation surrounding human orthologues of 459 mappable zebrafish DEGs and quantitative
229 ultrasound derived heel bone mineral density (eBMD) measured in 378,484 white European adults
230 (**figure 5A**). Strong evidence of enrichment was observed, suggesting that human orthologues of
231 zebrafish DEGs were on average more strongly associated with the eBMD than all other human protein
232 coding genes in the genome (β=0.20, SE=0.079, P=0.005, **table 2**). In a sensitivity analysis, we adjusted
233 further for the set of orthologues that could not be mapped between fish and humans, and for the
234 set of orthologues that was not expressed in ontogenetic and/or regenerating scales. Adjustment for
235 these potential confounders reduced the magnitude of enrichment by a third, however the set of DEGs
236 remained enriched for BMD associated orthologues (β=*0.14, SE=0.080, P=0.04*). Post hoc permutation
237 analysis suggested that enrichment was not attributable to all DEGs, but rather that a subset of DEGs
238 accounted for most of the enrichment. To further investigate this finding, DEGs were stratified
239 according to whether they were up- or downregulated, and each set was re-analysed. Enrichment for
240 BMD associated orthologues was stronger (β=0.27, SE=0.084, P=0.0006) for the 402 upregulated DEGs
241 and no evidence of enrichment was observed for the 57 downregulated DEGs (β=–0.31, SE=0.23,
242 P=0.91) (**figure S7A**). Subsequent post hoc analysis suggested that enrichment for BMD associated
243 orthologues was attributable to at least ~40% of the upregulated DEGs. We repeated the analysis
244 using height and osteoarthritis (OA) and observed evidence that DEGs were enriched for both
245 outcomes (P<0.005, **figure 5A**, **table 2, figure S7B**). Notably, post hoc analysis revealed that the
246 enrichment for height and OA associated human orthologues was not attributable to all DEGs.
247 Stratified analysis revealed that upregulated DEGs were more strongly enriched for height associated
248 orthologues, whereas the enrichment for OA associated genes remained largely unchanged (**figure**
249 **S7B, table 2**).
250
251 Finally, one advantage of MAGMA is that it first performs gene-based tests of associations between
252 each human protein coding gene in the genome, and the outcome of interest (see supplementary
253 methods for more detail). Consequently, once enrichment is observed we can prioritise orthologues
254 of DEGs for functional validation by comparing their relative strength of association with BMD, height
255 and/or OA (**figure 5C** and **data file S7**). Using this approach, we identified human orthologues of *spp1*
256 and *col11a2* that were both differentially upregulated in regenerating fish scales, and showed

257 different patterns of association with all three traits. Specifically *SPP1* was robustly associated with
258 BMD ($P=4\times10^{-15}$), but not height (P=0.16) or OA (P=0.16), whereas *COL11A2* was robustly associated
259 with height ($P=4.1\times10^{-13}$) and OA ($P=3.6\times10^{-7}$), but did not meet the stringent gene-wide significance
260 threshold of $P<2.63\times10^{-6}$ for BMD (i.e. $P=2.5\times10^{-3}$). Given these contrasting patterns of association,
261 together with the availability of the corresponding mutant zebrafish lines, we chose to further
262 investigate *spp1* and *col11a2* expression and establish whether mutant fish developed skeletal
263 abnormalities that were consistent with the above mentioned human genetic associations.

264 **Zebrafish mutants of differentially expressed genes show skeletal phenotypes consistent with**
265 **their expression profile and with human genetic associations**

266 Human orthologues of DEGS that had unique, or pleiotropic associations with eBMD, height and/or
267 OA were identified (**figure 5C**), and qRT-PCR was used to confirm that the corresponding DEGs
268 (including *spp1* and *col11a2*) were differentially expressed (**figure 6A**). We further assessed
269 transgenic reporter expression of *spp1* (*spp1:mCherry*) to determine gene expression localisation.
270 The expression pattern of *spp1:mCherry* was exclusively localised at the distal rim of the ontogenetic
271 scale, similar to *sp7:GFP* positive osteoblast localisation (**figure 6B**). Interestingly, these *sp7* positive
272 (sub)marginal cells at the rim are classed as more mesenchymal osteoblasts involved in *de novo*
273 bone formation in ontogenetic scales (Iwasaki, Kuroda et al., 2018). In regenerating scales, *sp7*
274 expression was seen more broadly but elevated at the posterior edge which was followed proximally
275 by an increased *spp1* signal with reduced *sp7* expression in the same area (**figure 6B**). The width of
276 *spp1* expression was increased compared to ontogenetic scales, implying an expansion of its activity
277 during bone growth and mineralisation in the regenerating scale (**figure 6C** and **6D**).

278 We next measured axial skeleton length from 3D micro-CT renders of *col11a2*$^{Y228X/Y228X}$ and
279 *spp1*$^{P160X/P160X}$ mutant zebrafish. This showed significant reduced length in *col11a2* mutants whilst
280 *spp1* mutants exhibited a milder tendency (**figure 7A**). Additionally, we segmented the lower jaw
281 (mandibular arch) and caudal vertebrae of these 3D micro-CT renders and measured several
282 histomorphological parameters using element landmarks as set out in **figure S8A-B**. These
283 measurements of the lower jaw demonstrated that *col11a2* fish have reduced width and length in
284 the lower jaw whereas *spp1* fish did not show significant changes (**figure 7B**). When we calculated
285 the ratio between length and width, both mutant lines showed a mild alteration in lower jaw
286 element proportion (**figure 7C**). Interestingly, in contrast to wildtype and *spp1* mutants, the *col11a2*
287 mutants exhibited altered joint shape consistent with the predicted OA phenotype in adulthood and
288 as seen in larval jaws previously (**figure 7D**)(Lawrence, Kague et al., 2018). Measurements of the
289 centrum, neural arch, and haemal arch of the vertebra did not show significant changes in either

290 mutant line (**figure 7E-G, figure S8C-G**) These histomorphological data show that indeed *col11a2* fish
291 showed bone growth defects while *spp1* mutants did not.

292 To test the prediction that *spp1* mutants would have abnormal BMD, we quantified mean volumetric
293 BMD from sites formed via different modes of ossification: the parietal plate of the cranium and the
294 first caudal vertebra as these are formed by intramembranous ossification and by ossification
295 directed by the notochord sheath, respectively. Consistent with our prediction, we observed an
296 increase in BMD for *spp1* mutants in both elements whereas no evidence of altered BMD was
297 observed for *col11a2* mutants (**figure 7H**). Interestingly, we observed a physical thickening of the
298 vertebral arches and anterior shaft of the vertebral centrum in *spp1* mutants consistent with the
299 relationship seen with the increased BMD (**figure 7G** and **figure S8E**). Taken together, our data
300 suggest that genes that are differentially expressed during scale regeneration play a role in wider
301 regulation of skeletal homeostasis at other skeletal sites in the zebrafish, and that mutants in these
302 genes have phenotypes that are largely consistent with those observed in humans.

303 *Discussion*

304 In this study we define, for the first time, the transcriptome of ontogenetic and regenerating zebrafish
305 scales and show that DEGs are enriched for biological pathways involved in osteoblast mediated bone
306 formation, many of which are conserved in humans. By integrating this information with large-scale
307 human genetic association studies, we show that human orthologues of DEGs were likely to play a
308 role in the pathogenesis of monogenic and polygenic human MSK disease. Our findings suggest that
309 zebrafish scale regeneration has the potential to help us better understand biological function and
310 pathways relevant to human skeletal health and disease.

311 Transcriptomic profiling revealed that regenerating scales predominantly upregulate gene
312 expression of many osteoblast genes, correlating with the high abundance of metabolically active
313 osteoblasts. The high expression of genes involved in ECM deposition, principally genes regulating
314 collagen synthesis, processing, and deposition fits with the regeneration of the collagen-rich matrix
315 of the bony scale. We demonstrated that while *col1a1a* is expressed throughout the regenerating
316 scale it is largely excluded from the leading edge labelled by *sp7.* By contrast, *col10a1a* is strongly
317 expressed in leading edge concomitant and newly forming lateral circuli that are associated with
318 thickening of the calcified matrix in accordance with the role of type X collagen as an early marker of
319 ossifying tissues in the zebrafish (Debiais-Thibaud, Simion et al., 2019, Eames, Amores et al., 2012,
320 Hammond & Schulte-Merker, 2009). Amongst DEG collagens, *col11a2* was one of the highest DEGs in
321 this profile. Interestingly, type XI collagen is more frequently associated with cartilage matrix
322 formation; interacting with type II collagen to regulate spacing and nucleation of fibrils in the ECM
323 (Gregory, Oxford et al., 2000, Li, Lacerda et al., 1995). As well as the collagens themselves, matrix
324 processing genes coding for MMPs were also upregulated. MMPs are important to breakdown the
325 dense type I collagen matrix and this process is crucial for tissue growth, shape, release and
326 distribution of signalling molecules, and cell migration (Page-McCaw, Ewald et al., 2007). We have
327 previously shown that *mmp9* is upregulated during scale regeneration and *mmp9* expression was
328 observed adjacent to newly deposited matrix and TRAP positive cells (de Vrieze et al., 2011).

329 Moreover, we observed transcriptional upregulation of ECM proteoglycans that bind collagens, such
330 as biglycan *(bgna/b*), which are important in regulating collagen nucleation and remodelling
331 (Douglas, Heinemann et al., 2006). Interestingly, biglycan has been shown to modulate ECM
332 accessibility and regulate diffusion of signalling molecules, such as Bmp4, regulating bone strength in
333 mice (Chen, Fisher et al., 2004, Xu, Bianco et al., 1998). Related to the abundant presence of collagen
334 related factors, cell adhesion genes, in particular integrin signalling, were enriched and connected to
335 the collagen and MMP networks. Cell adhesion and the ECM are interlinked and both must be tightly
336 regulated during rapid growth (Zeltz & Gullberg, 2016), such as osteogenic regeneration of the scale.

337 Cell adhesions are heavily modulated to allow cell rearrangements and tissue mechanics in
338 regenerative tissue expansion contexts. For example, in a mammalian epidermal wound healing
339 response it is crucial for epithelial regeneration (Mosaffa, Tetley et al., 2020).

340 Pathway analysis revealed signalling pathways related to ECM formation and expansion, such as
341 integrin, HH and IGF. The absence of enrichment (note these were also not under-represented) of
342 Wnt, Bmp, and Fgf pathway genes is likely to be associated with the timing of the transcriptomic
343 profile (9 dph). For example, it has been shown that Wnt and Fgf signalling are required for the
344 initiation of scale regeneration, with inhibiting Fgf or canonical Wnt signalling leading to a failure to
345 form scales (Aman, Fulbright et al., 2018). HH signalling controls morphogenesis of the scale over a
346 prolonged time period, where the HH ligand secreted from the epidermis regulates the rate of ECM
347 deposition by scale osteoblasts (Aman et al., 2018, Iwasaki et al., 2018).

348 Gene ontology analysis suggested that transcriptomic profiles of regenerating zebrafish scales were
349 enriched for biological pathways involved in bone formation and mineralisation. These pathways are
350 largely conserved in humans, prompting us to investigate whether DEGs were enriched for human
351 orthologues that cause human monogenic skeletal disorders, and that associate with polygenic MSK
352 traits and disease. Gene set analysis involving human genetic association studies complemented
353 findings from our gene ontology analysis, suggesting that DEGs were most strongly enriched for
354 human orthologues that cause monogenic disorders that were broadly characterised by abnormal or
355 decreased bone mineralisation, and separately, abnormal cartilage formation and bone growth.
356 Further analysis involving human polygenetic disease traits provided additional evidence that
357 upregulated (but not downregulated) DEGs, were enriched for human orthologues associated with
358 bone mineralisation as captured by heel bone ultrasound. Importantly, post hoc permutation analysis
359 revealed that although the set of upregulated DEGs was strongly enriched, it was likely that
360 enrichment was not attributable to all DEGS, but rather a nested subset (or subsets) of genes that
361 corresponded to one or more biological pathway(s) that regulates bone homeostasis in humans. A
362 possible explanation is that DEGs were identified using bulk RNA-sequencing, a method that captures
363 a heterogenous mixture of transcriptome signature profiles that define different cell types, states, and
364 their biological pathways, some of which may or may not be involved in bone mineralisation during
365 scale regeneration. Importantly, the small sample size of our transcriptomic study also limited our
366 ability to identify all DEGs and their associated biological pathways. However, as the scale contains a
367 heterogeneous cell population, this is the most likely cause of not identifying the nested subsets of
368 DEGs responsible for the enrichment. Hence, future studies may benefit by focusing on transcriptomic
369 profiling of separate cell populations from scales at different stages of regeneration to determine their
370 expression profiles to dissect the different pathways responsible for osteo-anabolic growth. This could

371 be achieved by, for example, using fluorescent automated cell sorting (FACS) to isolate various
372 populations using cell specific transgenic reporters (e.g. *sp7:GFP*) or even single cell RNA-seq
373 technologies to elucidate the transcriptional state of all different cell type populations in the
374 regenerating scale.

375 Given that DEGs appeared enriched for human orthologues associated with human MSK traits and
376 disease, we chose to perform detailed skeletal phenotyping on *spp1* and c*ol11a2* zebrafish mutants
377 to investigate whether they developed skeletal abnormalities that were consistent with their gene-
378 based associations with height, eBMD and/or OA. Both genes were upregulated DEGs in
379 regenerating scales and human orthologues of these genes showed contrasting patterns of
380 association with human disease traits (i.e. *SPP1* robustly associated with eBMD only*,* and *COL11A2*
381 robustly associated with height and OA, and suggestively associated with *BMD).* Mutant fish
382 developed skeletal abnormalities largely consistent with those predicted by the human genetic
383 association studies. Notably, in humans, mutations in *COL11A2* lead to Stickler syndrome, a
384 condition associated with craniofacial dysplasias, and joint abnormalities that lead to premature OA
385 (Couchouron & Masson, 2011). No clear human phenotype for *SPP1* (osteopontin) has been defined
386 yet, but it plays a complex role in regulating repair and regeneration of multiple tissues in
387 vertebrates. We show that *spp1:mCherry* was up-regulated in the regenerating scale adjacent to pre-
388 osteoblastic sp7+ cells which is consistent with previous reports that expression of *spp1* is up-
389 regulated during bone remodelling in both zebrafish fins and mammals (Morinobu, Ishijima et al.,
390 2003, Sousa, Valerio et al., 2012, Terai, Takano-Yamamoto et al., 1999). Moreover, *spp1* mutants
391 have elevated BMD in the cranial and axial endoskeleton, in line with murine studies where loss-of
392 *Spp1* leads to enhanced mineral content in some parts of trabecular bone (Boskey, Spevak et al.,
393 2002). Mouse studies have shown that *Spp1* determines mineralisation rate in the skeleton through
394 regulating *Phospho1* expression (Holm, Gleberzon et al., 2014, Yadav, Huesa et al., 2014). For
395 example, Osteopontin expression is detected during cranial suture closure in both mice and
396 zebrafish, suggesting a role in appropriate timing of pre-osteoblast differentiation (Kim, Lee et al.,
397 2003, Morinobu et al., 2003, Topczewska, Shoela et al., 2016). Outside of its function in skeletal
398 tissue, mammalian *Spp1* is functionally diverse, as it promotes angiogenesis and its expression is also
399 triggered during cutaneous wound healing to control the rate of repair (Dai, Peng et al., 2009, Mori,
400 Shaw et al., 2008). As *Spp1* is a component of the ECM and possesses integrin binding domains, it
401 can bind various integrins to modulate cell adhesion to the collagen matrix important during i.e.
402 tissue growth (Lamort, Giopanou et al., 2019). As we see high *spp1:mCherry* expression adjacent to
403 *sp7*+ pre-osteoblasts in the regenerating scale, it implies that *spp1* could play a role in differentiation

404 of these pre-osteoblasts and therefore timing of scale mineralisation and the association with
405 human eBMD is suggestive of a conserved function in control of BMD across species.

406 Since the prevalence of diseases with pronounced bone fragility phenotypes is increasing due to an
407 ageing population there is a need to discover and rapidly test new bone growth candidate genes that
408 could act as drug targets. These multi-factorial diseases have complex genetic and physiological
409 underpinnings that are not well understood, and as human bone samples are hard to obtain there is
410 a strong demand for models to study bone pathophysiology. The regenerating zebrafish scale could
411 therefore function as an additional model to study and discover osteo-anabolic factors relevant to
412 human skeletal diseases. The relative abundance of teleost scales (around 200 per fish) and their
413 amenability for imaging make them an ideal model for regenerative studies, and unlike caudal fins,
414 scales can be treated as independent bone units, each harbouring their native complex tissue
415 environment. Scales can be cultured *ex vivo* in a semi-high throughput multi-well format, offering an
416 avenue to test compounds that could complement established tissue culture and *in vivo*
417 pharmacology studies (Bergen et al., 2019, de Vrieze et al., 2015). By using a multi-disciplinary
418 approach we: i) described a transcriptomic profile of regenerating zebrafish scales, ii) showed that
419 DEGs are enriched for biological pathways involved in bone formation, and for genes associated with
420 MSK disease in human populations and, iii) studied mutant zebrafish for two DEGs and observed
421 skeletal abnormalities in both fish that were consistent with results from human genetic association
422 studies. In conclusion, we show that integrative analysis involving zebrafish transcriptomics and
423 human genetic association studies is feasable, and that future studies involving zebrafish scales have
424 potential to better our understanding of bone formation in general, and how defects in this complex
425 process contribute to musculoskeletal disease pathogenesis in humans.

426 *Material and Methods*
427

428 **Zebrafish husbandry, mutant and transgenic lines**

429 Zebrafish were maintained under normal husbandry conditions(Alestrom, D'Angelo et al., 2020).
430 Experiments were locally ethically reviewed (by AWERB at University of Bristol (Bristol, UK) (UoB)
431 and Radboud University (Nijmegen, NL) (RU) respectively) and performed under UK Home Office
432 project licence 30/3408 (UoB) or RU-DEC2014-059 (RU).

433 Wildtype AB/TL (UoB) and AB (RU) strains were used. Mutant lines (AB/TL background, UoB) have
434 been previously described; *col11a2*^{sa18324} carries a nonsense mutation causing a premature stop
435 codon at tyrosine position 228 (ENSDART00000151138.3), henceforth called *col11a2*^{Y228X} (Lawrence
436 et al., 2018) and *spp1*$^{CGAT327\text{-}330del}$ carrying a deletion leading to a frameshift resulting in a premature
437 stop codon nonsense mutation at proline position 160 (ENSDART00000101261.6), henceforth called
438 *spp1*^{P160X} (Bevan, Lim et al., 2020). Transgenic lines are listed in the **Supplemental Methods**.

439 **Elasmoid scale harvesting and imaging**

440 Anaesthetised fish (0.05% (v/v) tricaine methanesulfonate (MS-222) (UoB), 0.1% (v/v) 2-
441 phenoxyethanol (RU)) were put on a wet tissue containing system water and anaesthetic, and scales
442 plucked under a microscope with a watchmaker's tweezers from the midline of the lateral flanks
443 near the dorsal fin. Fluorescent microscope images of flanks (*in toto*) and single harvested scales (*in*
444 *situ*) were acquired on a fluorescent stereomicroscope (Leica Microsystems, Germany), using 2x, 4x,
445 and 8x magnification.

446 Adult fish were immersed in 40 µM Calcein (Sigma-Aldrich, cat# 154071-48-4) Danieau's buffer
447 solution (pH 7.4) for two hours and washed in system water for at least 15 minutes prior to imaging.

448 *Alkaline phosphatase staining*

449 Scales were collected in ALP buffer (100 mM Tris-HCl (pH 9.5), 100 mM NaCl, and 50 mM $MgCl_2$) and
450 stained in ALP buffer containing 2% (v/v) NBT/BCIP (Sigma, cat# 11681451001). After a brief wash in
451 deionised water, scales were mounted on a microscope slide containing 10 % (w/v) Mowiol® 4-88
452 (Sigma-Aldrich cat# 9002-89-5) in 25% (v/v) glycerol solution. Images were taken on an upright
453 microscope (Leica).

454 **RNA isolation, RNA sequencing, transcriptomic mapping and analysis**

455 Approximately 40 scales were collected from a standardized area on the left flank of 1-year old male
456 zebrafish; the area that extends from just behind the operculum to the implant of the dorsal fin. The

area may included multiple rows of scales of similar size and shape. Total RNA was isolated from ontogenetic and regenerating scales (n=3 fish per group, RU) by using Trizol (Invitrogen) for RNA-sequencing (RNA-seq) and downstream qRT-PCR testing.

RNA-seq was performed by ZF-GENOMICS (Leiden, NL) and involved quality control of total RNA libraries on 2100expert bioanalyzer (Agilent) that resulted in RIN scores of >9.2. Illumina RNAseq library preparation involved standard 6 nucleotide adaptor ligation. Paired single read 1 x 50 nucleotide runs (10 million reads; 0.5 Gb per sample) were performed on an Illumina Hiseq2500 system.

Transcriptome Mapping and Differential Expression Analysis

Raw reads were mapped to the GRCz11 primary assembly (Ensembl version 99) using STAR (version STAR_2.5.4b) software pipeline (Dobin, Davis et al., 2013). The read count table for all genes mapped was obtained from the mapping step and filtered to leave out lowly expressed genes by only keeping genes that had at least 5 mapped reads over all samples. The differential gene expression analysis was performed using the R-package DESeq2 (version 1.28.1)(Love, Huber et al., 2014) including the medians of ratio normalisation step to account for the bias in sequencing depth/coverage and RNA composition of samples. For determining DEGs, we used a threshold of 1.25 $\log_2$ fold (2.4-fold) change and a false discovery rate (FDR) of <0.05. Further details are in the **Supplemental Methods**.

For downstream analyses, genes were classed as 'expressed' in scales when all three ontogenetic and regenerating scale samples produced a >5 normalised read count (background gene list). Arbitrary threshold for differential expression was set at ±1.25 $\log_2$ fold and an adjusted p-value (padj) of ≤0.05 (DEG list).

Gene ontology enrichment and STRING network analysis

DEG and background expression gene lists' gene symbols were uploaded to GOrilla (Eden, Navon et al., 2009) using *Danio rerio* and 'two unranked lists of genes' as settings. The hierarchical images and Microsoft Excel files were used for figure making. Ensembl IDs of DEGs were analysed with an 'Overrepresentation Test' (Released 20200407) using Fisher's exact test and False Discovery Rate correction in PANTHER Gene Ontology (release 2020-06-01), and PANTHER 'Pathways' and 'Reactome pathways' (PANTHER version 15.0) software (Mi, Muruganujan et al., 2019).

For STRING (v11) gene network analysis (Szklarczyk, Gable et al., 2019), the DEG set (zebrafish gene symbols) was uploaded and interaction score (high, ≥0.7 or medium ≥0.4), number of interactions

488 (one shell with max. 10 interactions), and active interaction sources (all were on) were set. More
489 details are in the **Supplemental Methods**.

490 **Gene set enrichment analysis involving monogenic and polygenic skeletal traits and disease**
491 In conjunction with ISDS Nosology and Classification of Skeletal Disorders database (Mortier et al.,
492 2019), evidence of enrichment for human monogenic skeletal disease causing genes either total or
493 within each individual nosology-defined skeletal disorder groups) was performed using Fisher's Exact
494 Test of Independence as described in detail in the **Supplemental Methods** and (Youlten, Kemp et al.,
495 2020). Enrichment for polygenetic traits and disease was investigated using MAGMA competitive gene
496 set analysis. In the first stage zebrafish – human orthologues of all protein coding genes were mapped.
497 In the second stage, the strength association between each human protein coding gene and eBMD
498 and height and any form of self-reported or hospital defined OA was evaluated separately using the
499 weighted average of 3 different gene-based tests of association. Gene based tests of association were
500 performed using high quality genome-wide imputed genetic data (~12 million SNPs, INFO > 0.9, MAF
501 > 0.05%) from 378,484 white European adults from the UK-Biobank Study with eBMD and height
502 measures. For the analysis involving OA, publically available genome-wide association summary
503 results statistics were used instead of genome-wide imputed genotyping data (Tachmazidou,
504 Hatzikotoulas et al., 2019). In the final stage, competitive gene set analysis was used to compare the
505 mean strength of association of human orthologues of zebrafish DEGs with each trait / disease, to the
506 mean strength of association all other genes, and evidence of enrichment was quantified using a one-
507 sided test of statistical significance.
508 Sensitivity analysis was performed correcting for the set of human genes that could not be mapped
509 between human and zebrafish, and the set of human orthologues that was not expressed in zebrafish.
510 Finally, post hoc permutation analysis was performed for analyses that were suggestive of enrichment.
511 A detailed description of the methods is presented in the **Supplemental Methods**.

512 **Quantitative real-time PCR**
513 500ng of total RNA was treated with DNase (1 unit) and reverse-transcribed (random hexamer
514 primers) with SuperScript II (Invitrogen 100 units). iQ SYBR Green Supermix (Biorad) containing 350
515 nM primer and cDNA was used for amplification (primers and PCR conditions in **Supplemental**
516 **Methods**). Relative expression was calculated based on a normalisation index of two reference
517 genes: *eef1a1l1* and *rpl13*. For comparison of qRT-PCR and RNA-seq expression of amplicons, the
518 average of ontogenetic normalised expression (qRT-PCR) or read count (RNA-seq) were taken and
519 every individual value was compared to the average ontogenetic expression (e.g. read count
520 regenerating scales individual 2 / average read count ontogenetic). The p-values presented in the

521 figures were derived from a two-tailed t-test (qRT-PCR) and p-adjusted (padj) from the DESEQ2
522 analysis (RNA-seq).

523 **Micro-Computed Tomography and BMD calculations**

524 MicroCT was performed as previously described (Kague et al., 2019), with BMD calculated as
525 previously described (Stevenson et al., 2017). Briefly, adult WT sibling, *col11a2*^{Y228X} and *spp1*^{P160X}
526 mutant zebrafish (1 year old) were fixed, dehydrated to 70% EtOH and scanned at 21 µm voxel size
527 (scan settings 130 kV, 150 µA, 0.5-s exposure, 3141 projections). Images were reconstructed using
528 NRecon software (Version 1.7.1.0), with dynamic ranges calibrated against a scan of hydroxyapatite
529 phantoms (0.25 g.cm^{-3} and 0.75 g.cm^{-3}) scanned with identical parameters. For BMD calculations
530 Aviso software (Avison2020.2; Thermo Fisher Scientific) was used to isolate pixel greyscale values for
531 the skull (parietal) and vertebrae (vertebrae 11-13) and calibrated against the greyscale values of
532 known hydroxyapatite density phantoms (0.25 g.cm^{-3} and 0.75 g.cm^{-3}) to estimate mean BMD values
533 and their standard deviations. Histomorphological assessment of segmented jaw and vertebrae (11-
534 13) elements were determined by measuring the width, length, and depth of the elements (N.B. left
535 and right side of jaw elements were considered as independent measurements) in AVIZO between
536 element landmarks as shown in **figure S7A** and **7B**.

537 **Statistical testing**

538 All graphs and data of downstream RNA-seq functional data were analysed in GraphPad Prism (v
539 8.4.3) and were subjected to variance comparisons (F test) to determine distribution of the data
540 prior to performing an unpaired t-test comparing ontogenetic against regenerating or wildtype
541 against mutant conditions. P-values in figures as follows: n.s. >0.05, * ≤0.05, ** ≤0.01, *** ≤0.001.
542 RNA-seq, GO, STRING pathway, and GSEA statistical analyses are described in their relevant sections.

543 *Acknowledgements*
544 We would like to thank our funding sources: D.B. and C.H. received Fellowship funding from Versus
545 Arthritis (22044 and 21937 respectively). J.M. and G.F. were supported by the subsidy programme
546 Smartmix (SSM06010) of the Dutch Ministries of Economic Affairs and Education, Culture and,
547 Science. J.P.K was funded by a University of Queensland (UQ) Development Fellowship
548 (UQFEL1718945), a National Health and Medical Research Council (Australia) Investigator grant
549 (GNT1177938) and project grant (GNT1158758). M.L. is supported by a UQ Research Training
550 Scholarship and the Commonwealth Scientific and Industrial Research Organisation Postgraduate
551 Top-Up Scholarship. R.R. and R.J.R. were supported by the BHF Oxbridge Centre of Regenerative
552 Medicine (RM/17/2/33380) and a BHF Intermediate Fellowship to R.J.R. (FS/15/2/31225). This
553 research has been conducted using the UK Biobank Resource (accession ID: 53641). Lastly, we would
554 like to thank Mathew Green and Pablo Peon Garcia for fish care at UoB, and Tom Spanings and
555 Antoon van der Horst for fish care at RU.

556

557 *Author contributions*
558 D.B., and J.M. conceptualised and initiated the project. D.B., Q.T., J.P.K., CH., and J.M. designed the
559 experiments. D.B., Q.T., A.S, J.Z., E.N., J.P.K., M.L., S.Y., C.H., and J.M. performed the experiments
560 and analysed data. E.Z, S.Y., J.P.K, R.R. and R.J.R. provided reagents or access to datasets. D.B., J.P.K.,
561 C.H., and J.M. supervised the project. D.B., G.F. J.P.K., CH., and J.M. acquired funding for the project.
562 D.B. prepared manuscript figures. J.P.K, E.Z., S.Y, P.I.C., R.R., G.F. and R.J.R. provided expertise. D.B.,
563 J.P.K., C.H., and J.M. co-wrote the first version of the manuscript. All authors revised the first version
564 and approved the contents of the final version of the manuscript.

565 *Conflict of interest and ethics statement*
566 All authors declare no conflict of interest. Human genetic and animal research that is presented in
567 this work has been conducted with ethical approval as described in Material and Methods section.

568 *Data availability*
569 RNA-sequencing FASTQ files are available in ENA (https://www.ebi.ac.uk/ena) under accession
570 number PRJEB39971.

571 *Tables and Figures*

572

573 **Table 1: Top-40 smallest false discovery rate (FDR) differentially regulated transcripts (up (green)**
574 **and down (magenta) regulated in Log2 fold change) in regenerated scales (vs ontogenetic)**
575 **showing mean and standard deviation (Stdev) for each group (normalised read count).**

576

Ensembl ID	Gene symbol	Log_2 Fold Change	FDR	Gene description
ENSDARG00000068621	*si:ch211-181d7.3*	*-6.767*	2.41E-98	NOD-like receptor (NLR) with NACHT and LRR domain
ENSDARG00000074132	*scpp7*	3.756	2.83E-70	secretory calcium-binding phosphoprotein 7
ENSDARG00000093659	*entpd5b*	3.560	2.36E-48	ectonucleoside triphosphate diphosphohydrolase 5b
ENSDARG00000025089	*loxl4*	3.167	1.41E-47	lysyl oxidase-like 4
ENSDARG00000054753	*col10a1a*	3.610	3.10E-43	collagen, type X, alpha 1a
ENSDARG00000052633	*si:ch211-106n13.3*	4.676	7.84E-39	si:ch211-106n13.3
ENSDARG00000039999	*slc13a5b*	4.351	1.54E-37	solute carrier family 13 member 5b
ENSDARG00000012422	*col11a2*	3.484	6.80E-37	collagen, type XI, alpha 2
ENSDARG00000069216	*c6ast1*	4.275	1.02E-33	six-cysteine containing astacin protease 1
ENSDARG00000098226	*smpd3*	3.226	1.22E-32	sphingomyelin phosphodiesterase 3
ENSDARG00000004627	*panx3*	2.897	1.27E-27	pannexin 3
ENSDARG00000104267	*postnb*	2.775	1.18E-26	periostin, osteoblast specific factor b
ENSDARG00000024847	*col5a2b*	2.783	2.75E-26	collagen, type V, alpha 2b
ENSDARG00000009014	*col11a1b*	3.298	2.77E-26	collagen, type XI, alpha 1b
ENSDARG00000020007	*col1a2*	2.951	5.95E-26	collagen, type I, alpha 2
ENSDARG00000105153	*ifitm5*	3.133	1.29E-25	interferon induced transmembrane protein 5
ENSDARG00000042186	*paplnb*	3.405	7.38E-25	papilin b, proteoglycan-like sulfated glycoprotein
ENSDARG00000095259	*tmem119a*	2.622	6.06E-24	transmembrane protein 119a
ENSDARG00000088274	*si:ch211-181d7.1*	*-4.630*	6.06E-24	si:ch211-181d7.1
ENSDARG00000059746	*plod1a*	2.209	7.53E-24	procollagen-lysine, 2-oxoglutarate 5-dioxygenase 1a
ENSDARG00000115341	*col11a1a*	3.421	9.48E-24	collagen, type XI, alpha 1a
ENSDARG00000035809	*col1a1b*	2.926	1.34E-23	collagen, type I, alpha 1b
ENSDARG00000091667	*si:dkey-234i14.3*	3.501	3.99E-23	si:dkey-234i14.3
ENSDARG00000079572	*plcd3b*	3.515	1.50E-22	phospholipase C, delta 3b
ENSDARG00000058270	*si:ch211-114l13.7*	2.465	1.79E-22	si:ch211-114l13.7
ENSDARG00000055175	*c1qtnf6a*	3.482	2.61E-22	C1q and TNF related 6a
ENSDARG00000037145	*slc8a4b*	3.076	4.38E-21	solute carrier family 8 member 4b
ENSDARG00000101535	*col10a1b*	3.032	6.06E-21	collagen, type X, alpha 1b
ENSDARG00000078866	*sdk1a*	1.876	8.41E-21	sidekick cell adhesion molecule 1a
ENSDARG00000041703	*rrbp1b*	2.696	1.33E-20	ribosome binding protein 1b
ENSDARG00000040985	*itgbl1*	3.531	9.38E-20	integrin, beta-like 1
ENSDARG00000019949	*serpinh1b*	3.135	1.18E-19	serpin peptidase inhibitor, clade H (heat shock protein 47), member 1b
ENSDARG00000026348	*csad*	2.915	3.69E-19	cysteine sulfinic acid decarboxylase
ENSDARG00000012593	*col5a1*	2.447	5.67E-19	procollagen, type V, alpha 1
ENSDARG00000022437	*cd81b*	2.749	5.85E-19	CD81 molecule b
ENSDARG00000021265	*mybpc2b*	6.520	1.04E-18	myosin binding protein C, fast type b
ENSDARG00000009418	*mef2cb*	2.062	1.19E-18	myocyte enhancer factor 2cb
ENSDARG00000017884	*bgna*	2.896	3.32E-18	biglycan a
ENSDARG00000062363	*phex*	2.034	5.54E-18	phosphate regulating endopeptidase homolog, X-linked
ENSDARG00000079486	*fam20a*	2.263	1.12E-17	FAM20A golgi associated secretory pathway pseudokinase

577 **Table 2: MAGMA competitive gene set enrichment analysis with p-value of >0.05 in green.**

Model	Trait/Disease	#Genes	BETA	BETA STD	SE	P-value
ALL DEGs						
Base	**eBMD**	459	0.20	0.03	0.079	4.76E-03
	Height	459	0.35	0.05	0.102	3.18E-04
	Osteoarthritis	459	0.13	0.02	0.047	3.02E-03
Sensitivity	**eBMD**	459	0.14	0.02	0.080	4.02E-02
	Height	459	0.24	0.04	0.103	9.96E-03
	Osteoarthritis	459	0.12	0.02	0.048	6.91E-03
Upregulated DEGs						
Base	**eBMD**	402	0.27	0.04	0.084	5.61E-04
	Height	402	0.39	0.06	0.109	1.45E-04
	Osteoarthritis	402	0.14	0.02	0.050	3.26E-03
Sensitivity	**eBMD**	402	0.21	0.03	0.085	6.57E-03
	Height	402	0.29	0.04	0.110	4.56E-03
	Osteoarthritis	402	0.12	0.02	0.051	7.05E-03
Downregulated DEGs						
Base	**eBMD**	57	-0.31	-0.02	0.227	9.13E-01
	Height	57	0.01	0.00	0.292	4.86E-01
	Osteoarthritis	57	0.07	0.00	0.131	2.89E-01
Sensitivity	**eBMD**	57	-0.38	-0.02	0.228	9.53E-01
	Height	57	-0.10	-0.01	0.292	6.38E-01
	Osteoarthritis	57	0.06	0.00	0.131	3.29E-01
Key: described in supplemental data file S7						

Bergen et al _ Figure 1

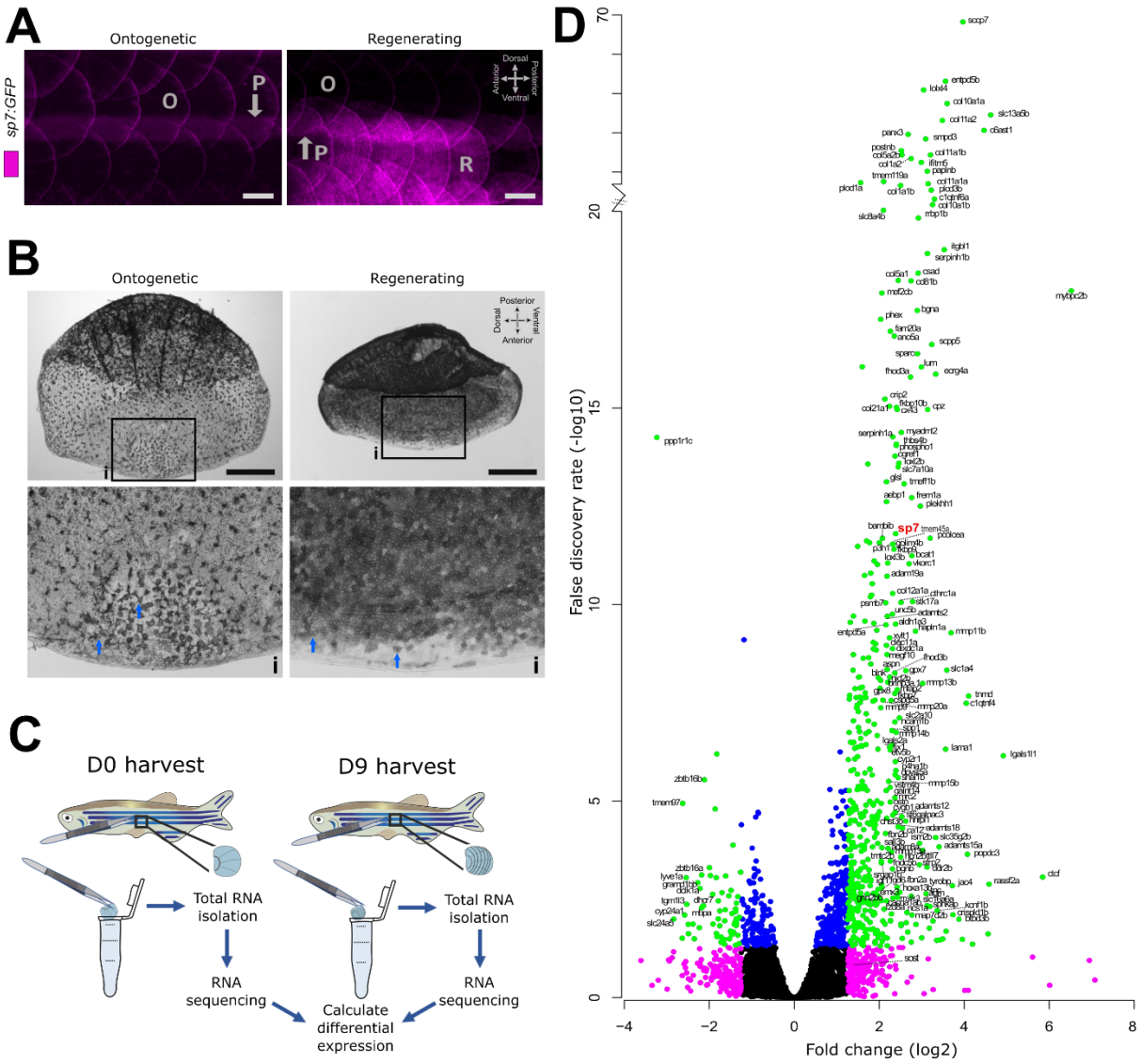

580

581 **Figure 1: RNA-sequencing transcriptomics of ontogenetic and 9 days regenerated scales. A)** *In toto*
582 fluorescent stereomicroscope images of flanks from *sp7:GFP* transgenic fish showing ontogenetic (O)
583 and regenerated scales (R) in an anterior (left) to posterior (right) direction). Note the auto-
584 fluorescent pigment stripe (P) and the compass orientation is used to depict *in toto* scales in this
585 paper with the distal (posterior) edge pointing caudally. **B)** *In situ* alkaline phosphatase staining of a
586 pre-collection and 8 dph scale with insets (i) showing anterior part of the scale. Blue arrows indicate
587 ALP+ cells which appear to be larger and more extended in ontogenetic than regenerating scales.
588 Compass orientation is used to depict *in situ* scales in this paper as the anterior region was closest to
589 the scale dermal socket (pre-harvest). **C)** Schematic drawing of the RNA-sequencing approach. **D)**
590 Volcano plot showing relative fold change (log_2) and false discovery rate ($-log_{10}$ converted) of coding
591 RNA sequences expressed in both ontogenetic and regenerating scales. Green (≥±1.25 fold change, ≥
592 1.3 FDR), magenta (≥±1.25 fold change, <1.3 FDR), blue (<±1.25 fold change, ≥1.3 FDR), and black
593 (not passing any threshold) coloured dots mark the different criteria.

594

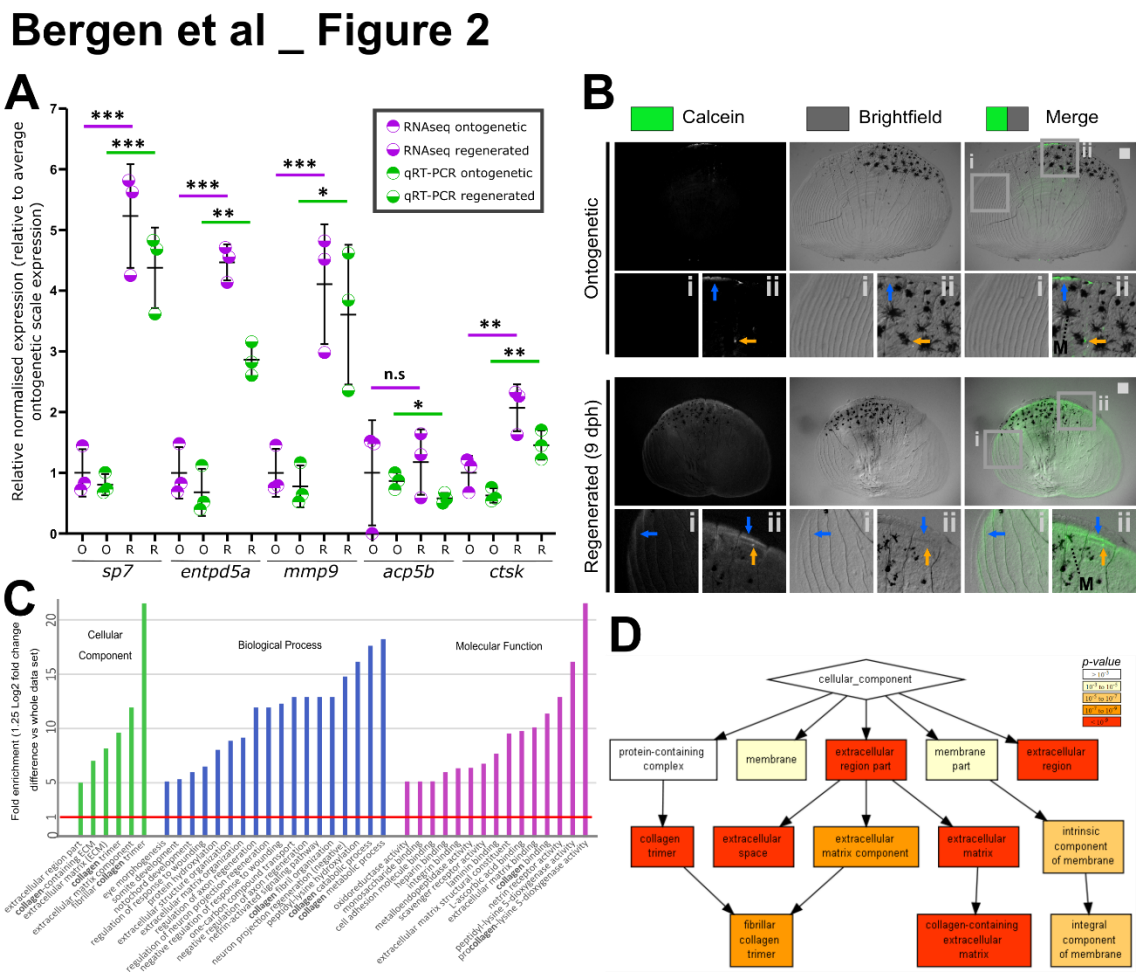

Figure 2: Validation and gene ontology of RNA-sequencing dataset. A) Comparison of relative expression levels of quantitative real-time PCR (qRT-PCR) and transcriptomic analysis of selected amplicons. **B)** Representative stereomicroscope images of live calcein green staining labelling newly deposited calcium phosphate of ontogenetic and regenerating scales (n = 4 fish each condition). Blue arrow indicates elevated levels of calcein green labelling compared to surrounding signal whereas orange arrows indicate small puncta of enhanced signal. Insets show lateral circuli (i) and posterior epidermal (containing pigmentating melanocytes (M) region (ii). **C)** GOrilla Gene ontology (GO) analysis showing high enrichment (>5 fold) of collagen and ECM related terms. **D)** GOrilla cellular component hierarchical clustering. Scale bar: 100 µm.

Bergen et al _ Figure 3

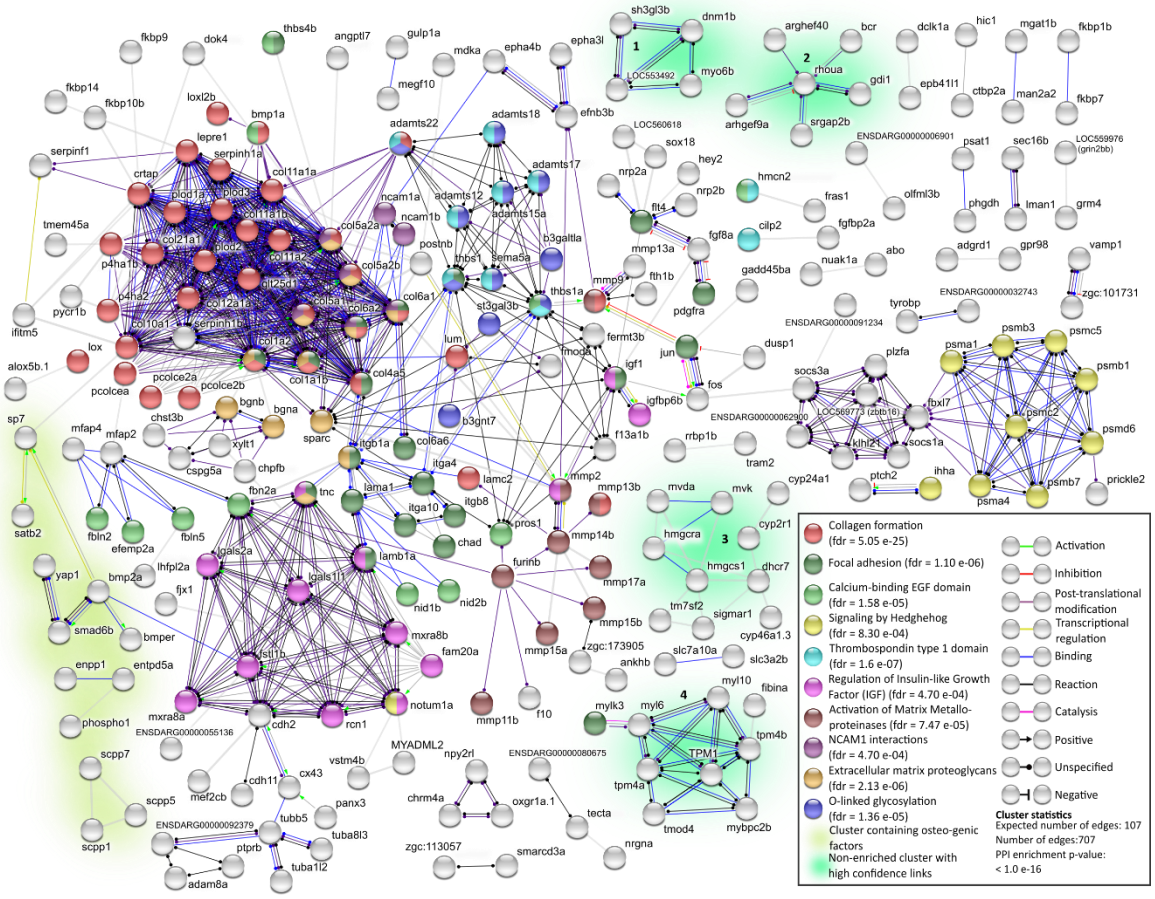

606

607 **Figure 3: STRING network analysis of DEGs.** Only DEG proteins with 1 or more protein-protein
608 interactions (PPI) (indicated as edges) were shown.

609

Bergen et al _ Figure 4

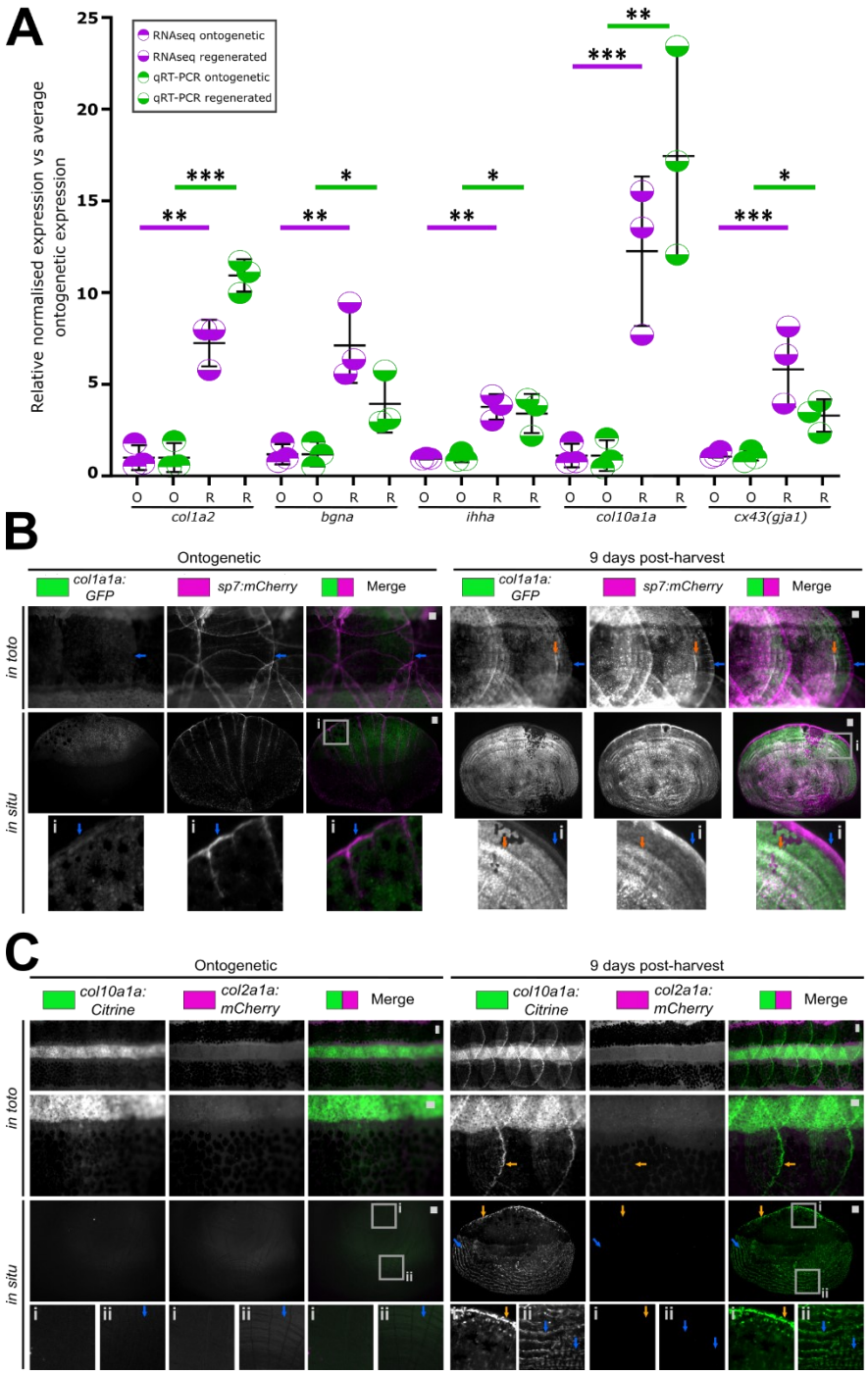

Figure 4: Validation of gene ontology findings. A) Relative expression levels of qRT-PCR and transcriptomic analysis of amplicons found in the collagen, proteoglycan and hedgehog signalling networks. **B)** Images of *in toto* and harvested scales (*in situ*) of *col1a1a:GFP* and *sp7:mCherry-NTR* double transgenic fish (n = 4 each condition). Blue arrow indicates the posterior (distal) fringe with high expression of mCherry. Orange arrow points at co-expression of GFP and mCherry. **C)** *In toto* and *in situ* stereomicroscope images of *col10a1a:Citrine* and *col2a1a:mCherry* double transgenic ontogenetic and regenerating scales (n = 4 fish each condition). Orange arrow indicate Citrine signal

618 at the posterior distal edge (inset i) while blue arrow points at a newly forming lateral circulus (inset
619 ii) of the scale. Scale bar: 100 µm.

620

Bergen et al _ Figure 5

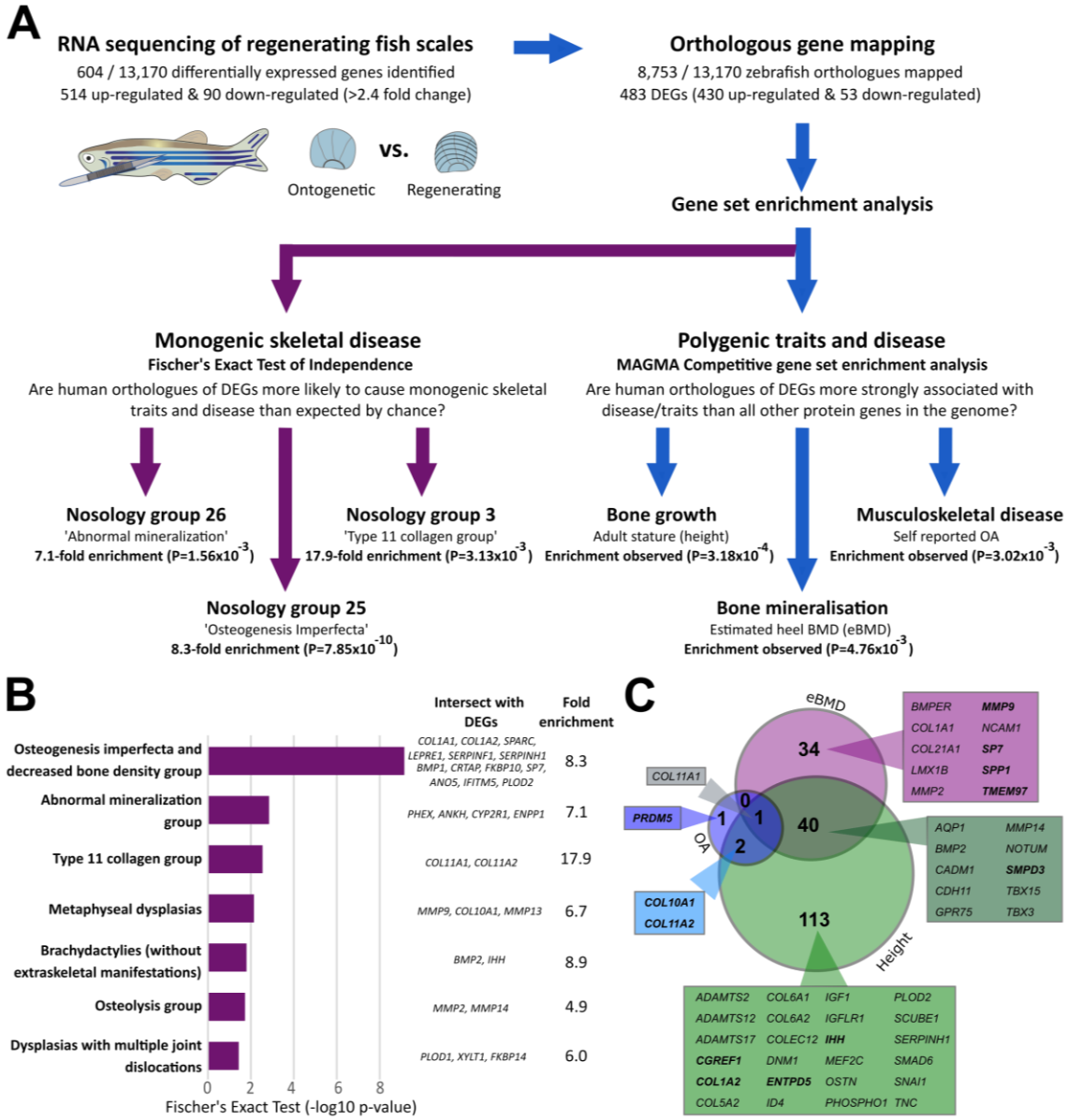

Figure 5: Gene set enrichment analysis strategy showing gene set enrichment of zebrafish DEGs in monogenic skeletal disorders and complex musculoskeletal traits and disease. A) Flow diagram summarising gene set enrichment analysis approach showing examples of enriched monogenic nosology groups and polygenic traits using human orthologues of zebrafish DEGs. **B)** Graph showing p-value of monogenic skeletal dysplasia nosology groups found in this study. The fold enrichment and human disease genes and zebrafish DEGs intersect are listed as well. **C)** Venn diagram of gene-based tests of association post-hoc analysis output showing number of associated DEGs with a stringent gene-wide significance threshold of $P<2.63\times10^{-6}$. The diagrams show the unique or intersecting genes between estimated bone mineral density (eBMD), osteoarthritis (OA), and height UK-Biobank gene based tests of association. The boxes show selected examples of DEG in each category and bold gene symbols are validated in this study.

Bergen et al _ Figure 6

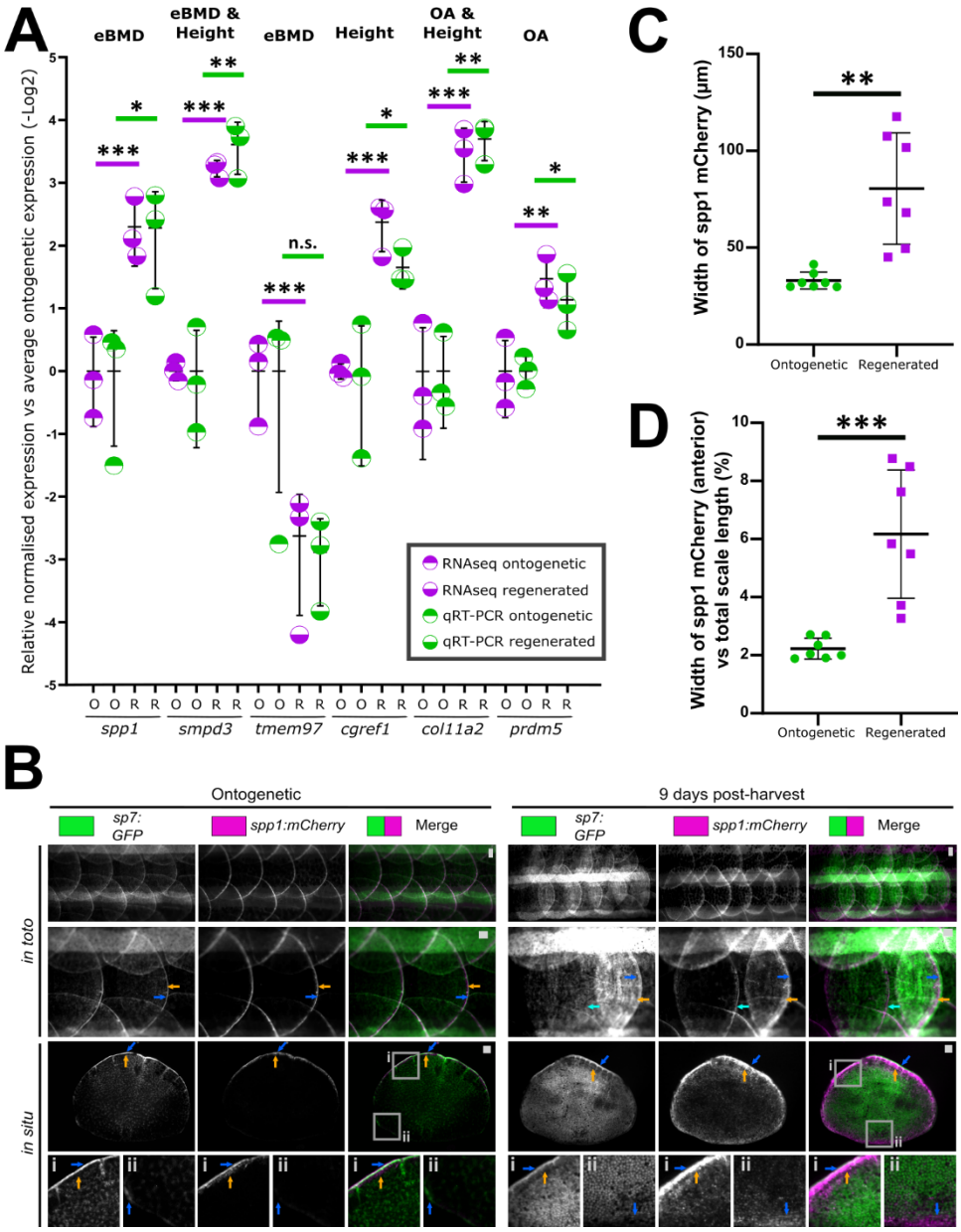

Figure 6: Validation of genes associated with polygenic traits in humans. A) Q-RTPCR and RNA-seq expression levels (relative to average ontogenetic expression) of selected DEG found in each category. All but one (*tmem97*) reached statistical threshold of p<0.05. **B)** Images of scales from *in toto* and harvested scales of *sp7:GFP* and *spp1:mCherry* double transgenic fish (ontogenetic: n = 5, regenerating: n = 4 fish). For overview and inset i, blue arrows indicate high GFP signal and orange the mCherry signal at the posterior edge (inset i) while light blue arrow indicates an ontogenetic scale next to a regenerating scale. Inset ii shows anterior region of the scale with opposite GFP and mCherry signals (blue arrow) in ontogenetic and regenerating conditions. **C)** Quantification of width of the mCherry signal at the posterior edge from harvested scales (between blue and orange arrows in panel C). **D)** Width of mCherry signal normalised by scale length (anterior to posterior). Scale bar: 100 µm.

Bergen et al _ Figure 7

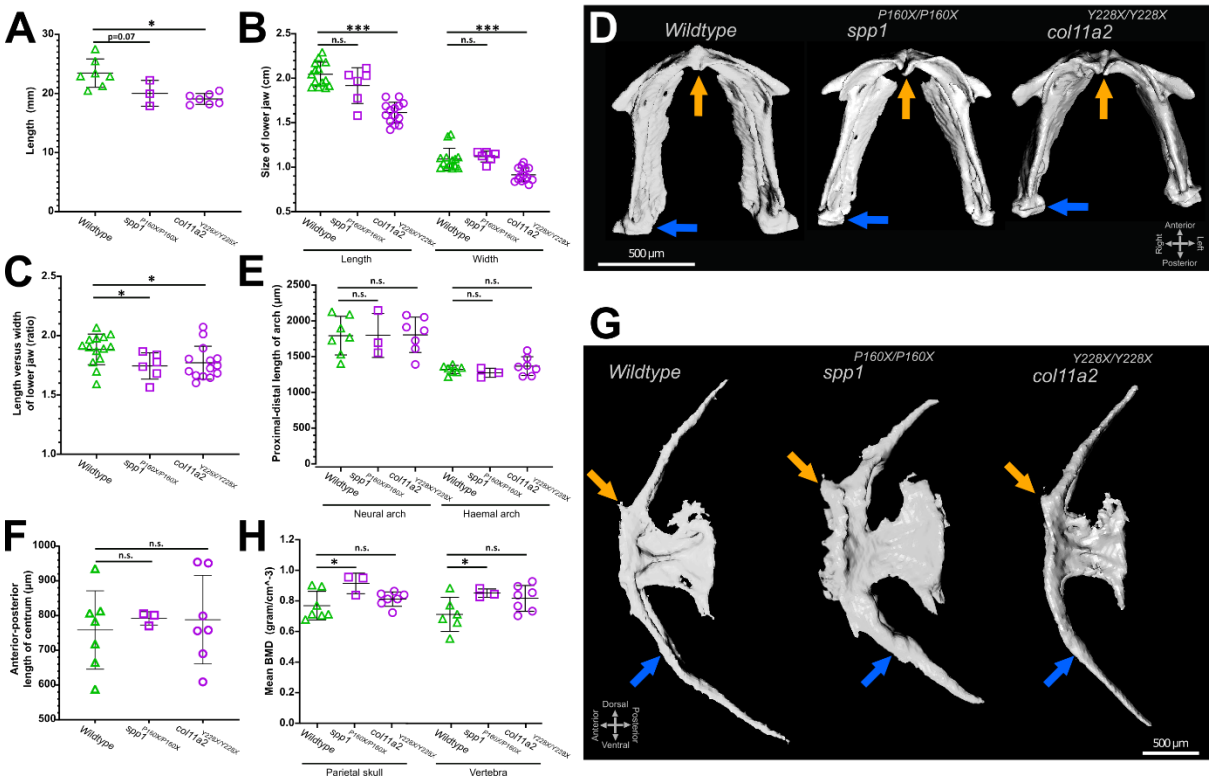

Figure 7: Histomorphology and bone mineral density measurements on 3D micro-CT images of *col11a2*^{Y228X} and *spp1*^{P160X} homozygous fish revealed altered bone structures. A) Axial skeleton length was reduced in *col11a2* mutants whereas *spp1* mutants showed a mild reduced tendency. **B)** Quantification of lower jaw size. **B)** Calculation of lower jaw element proportions. **D)** Ventral view of the segmented lower jaw images. Orange arrow indicates anterior mandibular arch joint and blue arrow shows mandibular arch – palatoquadrate (not visible) joint. **E)** Quantification of the vertebral arches' length. **F)** Total length of the anterior facet of the vertebral centrum. **G)** Lateral view of segmented images of the first caudal vertebra showing the anterior facet (orange arrow) and haemal arch (blue arrow). **H)** Mean BMD calculations of dermal and notochord sheath derived bone.

References

Alestrom P, D'Angelo L, Midtlyng PJ, Schorderet DF, Schulte-Merker S, Sohm F, Warner S (2020) Zebrafish: Housing and husbandry recommendations. *Lab Anim* 54: 213-224

Aman AJ, Fulbright AN, Parichy DM (2018) Wnt/β-catenin regulates an ancient signaling network during zebrafish scale development. *eLife* 7: e37001

Balemans W, Ebeling M, Patel N, Van Hul E, Olson P, Dioszegi M, Lacza C, Wuyts W, Van Den Ende J, Willems P, Paes-Alves AF, Hill S, Bueno M, Ramos FJ, Tacconi P, Dikkers FG, Stratakis C, Lindpaintner K, Vickery B, Foernzler D et al. (2001) Increased bone density in sclerosteosis is due to the deficiency of a novel secreted protein (SOST). *Human Molecular Genetics* 10: 537-544

Bereiter-Hahn J, Zylberberg L (1993) Regeneration of teleost fish scale. *Comparative Biochemistry and Physiology Part A: Physiology* 105: 625-641

Bergen DJM, Kague E, Hammond CL (2019) Zebrafish as an Emerging Model for Osteoporosis: A Primary Testing Platform for Screening New Osteo-Active Compounds. *Front Endocrinol (Lausanne)* 10: 6

Bevan L, Lim ZW, Venkatesh B, Riley PR, Martin P, Richardson RJ (2020) Specific macrophage populations promote both cardiac scar deposition and subsequent resolution in adult zebrafish. *Cardiovasc Res* 116: 1357-1371

Bhattacharya S, Hyland C, Falk MM, Iovine MK (2020) Connexin 43 gap junctional intercellular communication inhibits evx1 expression and joint formation in regenerating fins. *Development* 147: dev190512

Bigi A, Burghammer M, Falconi R, Koch MHJ, Panzavolta S, Riekel C (2001) Twisted Plywood Pattern of Collagen Fibrils in Teleost Scales: An X-ray Diffraction Investigation. *Journal of Structural Biology* 136: 137-143

Boskey AL, Spevak L, Paschalis E, Doty SB, McKee MD (2002) Osteopontin Deficiency Increases Mineral Content and Mineral Crystallinity in Mouse Bone. *Calcified Tissue International* 71: 145-154

Carnovali M, Luzi L, Banfi G, Mariotti M (2016) Chronic hyperglycemia affects bone metabolism in adult zebrafish scale model. *Endocrine* 54: 808-817

Carnovali M, Ottria R, Pasqualetti S, Banfi G, Ciuffreda P, Mariotti M (2016) Effects of bioactive fatty acid amide derivatives in zebrafish scale model of bone metabolism and disease. *Pharmacological Research* 104: 1-8

Chen X-D, Fisher LW, Robey PG, Young MF (2004) The small leucine-rich proteoglycan biglycan modulates BMP-4-induced osteoblast differentiation. *The FASEB Journal* 18: 948-958

Cosman F, Crittenden DB, Adachi JD, Binkley N, Czerwinski E, Ferrari S, Hofbauer LC, Lau E, Lewiecki EM, Miyauchi A, Zerbini CAF, Milmont CE, Chen L, Maddox J, Meisner PD, Libanati C, Grauer A (2016) Romosozumab Treatment in Postmenopausal Women with Osteoporosis. *New England Journal of Medicine* 375: 1532-1543

Couchouron T, Masson C (2011) Early-onset progressive osteoarthritis with hereditary progressive ophtalmopathy or Stickler syndrome. *Joint Bone Spine* 78: 45-49

Cox BD, De Simone A, Tornini VA, Singh SP, Di Talia S, Poss KD (2018) In Toto Imaging of Dynamic Osteoblast Behaviors in Regenerating Skeletal Bone. *Current Biology* 28: 3937-3947.e4

Dai J, Peng L, Fan K, Wang H, Wei R, Ji G, Cai J, Lu B, Li B, Zhang D, Kang Y, Tan M, Qian W, Guo Y (2009) Osteopontin induces angiogenesis through activation of PI3K/AKT and ERK1/2 in endothelial cells. *Oncogene* 28: 3412-3422

de Vrieze E, Sharif F, Metz JR, Flik G, Richardson MK (2011) Matrix metalloproteinases in osteoclasts of ontogenetic and regenerating zebrafish scales. *Bone* 48: 704-712

de Vrieze E, van Kessel MA, Peters HM, Spanings FA, Flik G, Metz JR (2014) Prednisolone induces osteoporosis-like phenotype in regenerating zebrafish scales. *Osteoporos Int* 25: 567-78

de Vrieze E, Zethof J, Schulte-Merker S, Flik G, Metz JR (2015) Identification of novel osteogenic compounds by an ex-vivo sp7:luciferase zebrafish scale assay. *Bone* 74: 106-113

706 Debiais-Thibaud M, Simion P, Ventéo S, Muñoz D, Marcellini S, Mazan S, Haitina T (2019) Skeletal
707 Mineralization in Association with Type X Collagen Expression Is an Ancestral Feature for Jawed
708 Vertebrates. *Molecular Biology and Evolution* 36: 2265-2276
709 Dhouailly D, Godefroit P, Martin T, Nonchev S, Caraguel F, Oftedal O (2019) Getting to the root of
710 scales, feather and hair: As deep as odontodes? *Experimental Dermatology* 28: 503-508
711 Dobin A, Davis CA, Schlesinger F, Drenkow J, Zaleski C, Jha S, Batut P, Chaisson M, Gingeras TR (2013)
712 STAR: ultrafast universal RNA-seq aligner. *Bioinformatics* 29: 15-21
713 Douglas T, Heinemann S, Bierbaum S, Scharnweber D, Worch H (2006) Fibrillogenesis of collagen
714 types I, II, and III with small leucine-rich proteoglycans decorin and biglycan. *Biomacromolecules* 7:
715 2388-93
716 Eames BF, Amores A, Yan Y-L, Postlethwait JH (2012) Evolution of the osteoblast: skeletogenesis in
717 gar and zebrafish. *BMC Evolutionary Biology* 12: 27
718 Eden E, Navon R, Steinfeld I, Lipson D, Yakhini Z (2009) GOrilla: a tool for discovery and visualization
719 of enriched GO terms in ranked gene lists. *BMC Bioinformatics* 10: 48-48
720 Giraud-Guille MM (1988) Twisted plywood architecture of collagen fibrils in human compact bone
721 osteons. *Calcified Tissue International* 42: 167-180
722 Gregory KE, Oxford JT, Chen Y, Gambee JE, Gygi SP, Aebersold R, Neame PJ, Mechling DE, Bächinger
723 HP, Morris NP (2000) Structural Organization of Distinct Domains within the Non-collagenous N-
724 terminal Region of Collagen Type XI. *Journal of Biological Chemistry* 275: 11498-11506
725 Guellec DL, Zylberberg L (1998) Expression of Type I and Type V Collagen mRNAs in the Elasmoid
726 Scales of a Teleost Fish as Revealed by In Situ Hybridization. *Connective Tissue Research* 39: 257-267
727 Hammond CL, Schulte-Merker S (2009) Two populations of endochondral osteoblasts with
728 differential sensitivity to Hedgehog signalling. *Development* 136: 3991-4000
729 Holm E, Gleberzon Jared S, Liao Y, Sørensen Esben S, Beier F, Hunter Graeme K, Goldberg Harvey A
730 (2014) Osteopontin mediates mineralization and not osteogenic cell development in vitro.
731 *Biochemical Journal* 464: 355-364
732 Iwasaki M, Kuroda J, Kawakami K, Wada H (2018) Epidermal regulation of bone morphogenesis
733 through the development and regeneration of osteoblasts in the zebrafish scale. *Developmental*
734 *Biology* 437: 105-119
735 Kenkre JS, Bassett JHD (2018) The bone remodelling cycle. *Annals of Clinical Biochemistry* 55: 308-
736 327
737 Kim H-J, Lee M-H, Park H-S, Park M-H, Lee S-W, Kim S-Y, Choi J-Y, Shin H-I, Kim H-J, Ryoo H-M (2003)
738 Erk pathway and activator protein 1 play crucial roles in FGF2-stimulated premature cranial suture
739 closure. *Developmental Dynamics* 227: 335-346
740 Kobayashi-Sun J, Yamamori S, Kondo M, Kuroda J, Ikegame M, Suzuki N, Kitamura KI, Hattori A,
741 Yamaguchi M, Kobayashi I (2020) Uptake of osteoblast-derived extracellular vesicles promotes the
742 differentiation of osteoclasts in the zebrafish scale. *Commun Biol* 3: 190
743 Lamort A-S, Giopanou I, Psallidas I, Stathopoulos GT (2019) Osteopontin as a Link between
744 Inflammation and Cancer: The Thorax in the Spotlight. *Cells* 8: 815
745 Lawrence EA, Kague E, Aggleton JA, Harniman RL, Roddy KA, Hammond CL (2018) The mechanical
746 impact of col11a2 loss on joints; col11a2 mutant zebrafish show changes to joint development and
747 function, which leads to early-onset osteoarthritis. *Philosophical Transactions of the Royal Society B:*
748 *Biological Sciences* 373: 20170335
749 Li X, Ominsky MS, Niu Q-T, Sun N, Daugherty B, D'Agostin D, Kurahara C, Gao Y, Cao J, Gong J,
750 Asuncion F, Barrero M, Warmington K, Dwyer D, Stolina M, Morony S, Sarosi I, Kostenuik PJ, Lacey
751 DL, Simonet WS et al. (2008) Targeted Deletion of the Sclerostin Gene in Mice Results in Increased
752 Bone Formation and Bone Strength. *Journal of Bone and Mineral Research* 23: 860-869
753 Li Y, Lacerda DA, Warman ML, Beier DR, Yoshioka H, Ninomiya Y, Oxford JT, Morris NP,
754 Andrikopoulos K, Ramirez F, Wardell BB, Lifferth GD, Teuscher C, Woodward SR, Taylor BA,
755 Seegmiller RE, Olsen BR (1995) A fibrillar collagen gene, Col11a1, is essential for skeletal
756 morphogenesis. *Cell* 80: 423-430

Lleras-Forero L, Winkler C, Schulte-Merker S (2020) Zebrafish and medaka as models for biomedical research of bone diseases. *Developmental Biology* 457: 191-205

Long F, Ornitz DM (2013) Development of the endochondral skeleton. *Cold Spring Harbor perspectives in biology* 5: a008334

Love MI, Huber W, Anders S (2014) Moderated estimation of fold change and dispersion for RNA-seq data with DESeq2. *Genome Biology* 15: 550

Mi H, Muruganujan A, Ebert D, Huang X, Thomas PD (2019) PANTHER version 14: more genomes, a new PANTHER GO-slim and improvements in enrichment analysis tools. *Nucleic Acids Research* 47: D419-D426

Mori R, Shaw TJ, Martin P (2008) Molecular mechanisms linking wound inflammation and fibrosis: knockdown of osteopontin leads to rapid repair and reduced scarring. *J Exp Med* 205: 43-51

Morinobu M, Ishijima M, Rittling SR, Tsuji K, Yamamoto H, Nifuji A, Denhardt DT, Noda M (2003) Osteopontin Expression in Osteoblasts and Osteocytes During Bone Formation Under Mechanical Stress in the Calvarial Suture In Vivo. *Journal of Bone and Mineral Research* 18: 1706-1715

Mortier GR, Cohn DH, Cormier-Daire V, Hall C, Krakow D, Mundlos S, Nishimura G, Robertson S, Sangiorgi L, Savarirayan R, Sillence D, Superti-Furga A, Unger S, Warman ML (2019) Nosology and classification of genetic skeletal disorders: 2019 revision. *American Journal of Medical Genetics Part A* 179: 2393-2419

Mosaffa P, Tetley RJ, Rodríguez-Ferran A, Mao Y, Muñoz JJ (2020) Junctional and cytoplasmic contributions in wound healing. *Journal of The Royal Society Interface* 17: 20200264

Padhi BK, Joly L, Tellis P, Smith A, Nanjappa P, Chevrette M, Ekker M, Akimenko M-A (2004) Screen for genes differentially expressed during regeneration of the zebrafish caudal fin. *Developmental Dynamics* 231: 527-541

Page-McCaw A, Ewald AJ, Werb Z (2007) Matrix metalloproteinases and the regulation of tissue remodelling. *Nature Reviews Molecular Cell Biology* 8: 221-233

Pasqualetti S, Banfi G, Mariotti M (2012) The zebrafish scale as model to study the bone mineralization process. *Journal of Molecular Histology* 43: 589-595

Pasqualetti S, Congiu T, Banfi G, Mariotti M (2015) Alendronate rescued osteoporotic phenotype in a model of glucocorticoid-induced osteoporosis in adult zebrafish scale. *Int J Exp Pathol* 96: 11-20

Pathak JL, Bravenboer N, Klein-Nulend J (2020) The Osteocyte as the New Discovery of Therapeutic Options in Rare Bone Diseases. *Frontiers in endocrinology* 11: 405-405

Ricard-Blum S (2011) The collagen family. *Cold Spring Harbor perspectives in biology* 3: a004978

Richardson R, Slanchev K, Kraus C, Knyphausen P, Eming S, Hammerschmidt M (2013) Adult Zebrafish as a Model System for Cutaneous Wound-Healing Research. *Journal of Investigative Dermatology* 133: 1655-1665

Schmidt JR, Geurtzen K, von Bergen M, Schubert K, Knopf F (2019) Glucocorticoid Treatment Leads to Aberrant Ion and Macromolecular Transport in Regenerating Zebrafish Fins. *Frontiers in Endocrinology* 10

Sehring IM, Weidinger G (2020) Recent advancements in understanding fin regeneration in zebrafish. *WIREs Developmental Biology* 9: e367

Shimada A, Kawanishi T, Kaneko T, Yoshihara H, Yano T, Inohaya K, Kinoshita M, Kamei Y, Tamura K, Takeda H (2013) Trunk exoskeleton in teleosts is mesodermal in origin. *Nature Communications* 4: 1639

Sire JY, Akimenko MA (2004) Scale development in fish: a review, with description of sonic hedgehog (shh) expression in the zebrafish (Danio rerio). *Int J Dev Biol* 48: 233-47

Sire JY, Allizard F, Babiar O, Bourguignon J, Quilhac A (1997) Scale development in zebrafish (Danio rerio). *Journal of anatomy* 190 (Pt 4): 545-561

Sire JY, Donoghue PC, Vickaryous MK (2009) Origin and evolution of the integumentary skeleton in non-tetrapod vertebrates. *J Anat* 214: 409-40

Sousa S, Valerio F, Jacinto A (2012) A new zebrafish bone crush injury model. *Biology open* 1: 915-21

807 Szklarczyk D, Gable AL, Lyon D, Junge A, Wyder S, Huerta-Cepas J, Simonovic M, Doncheva NT,
808 Morris JH, Bork P, Jensen LJ, Mering Cv (2019) STRING v11: protein-protein association networks
809 with increased coverage, supporting functional discovery in genome-wide experimental datasets.
810 *Nucleic acids research* 47: D607-D613
811 Tachmazidou I, Hatzikotoulas K, Southam L, Esparza-Gordillo J, Haberland V, Zheng J, Johnson T,
812 Koprulu M, Zengini E, Steinberg J, Wilkinson JM, Bhatnagar S, Hoffman JD, Buchan N, Süveges D, arc
813 OC, Yerges-Armstrong L, Smith GD, Gaunt TR, Scott RA et al. (2019) Identification of new therapeutic
814 targets for osteoarthritis through genome-wide analyses of UK Biobank data. *Nature genetics* 51:
815 230-236
816 Terai K, Takano-Yamamoto T, Ohba Y, Hiura K, Sugimoto M, Sato M, Kawahata H, Inaguma N,
817 Kitamura Y, Nomura S (1999) Role of Osteopontin in Bone Remodeling Caused by Mechanical Stress.
818 *Journal of Bone and Mineral Research* 14: 839-849
819 Topczewska JM, Shoela RA, Tomaszewski JP, Mirmira RB, Gosain AK (2016) The Morphogenesis of
820 Cranial Sutures in Zebrafish. *PLoS One* 11: e0165775-e0165775
821 Wu XM, Chen WQ, Hu YW, Cao L, Nie P, Chang MX (2018) RIP2 Is a Critical Regulator for NLRs
822 Signaling and MHC Antigen Presentation but Not for MAPK and PI3K/Akt Pathways. *Frontiers in*
823 *Immunology* 9
824 Xu T, Bianco P, Fisher LW, Longenecker G, Smith E, Goldstein S, Bonadio J, Boskey A, Heegaard A-M,
825 Sommer B, Satomura K, Dominguez P, Zhao C, Kulkarni AB, Robey PG, Young MF (1998) Targeted
826 disruption of the biglycan gene leads to an osteoporosis-like phenotype in mice. *Nature Genetics* 20:
827 78-82
828 Yadav MC, Huesa C, Narisawa S, Hoylaerts MF, Moreau A, Farquharson C, Millán JL (2014) Ablation
829 of osteopontin improves the skeletal phenotype of phospho1(-/-) mice. *J Bone Miner Res* 29: 2369-
830 2381
831 Yasuo M (1980) The source of calcium in regenerating scales of the goldfish, Carassius auratus.
832 *Comparative Biochemistry and Physiology Part A: Physiology* 66: 521-524
833 Youlten SE, Kemp JP, Logan JG, Ghirardello EJ, Sergio CM, Dack MRG, Guilfoyle SE, Leitch VD,
834 Butterfield NC, Komla-Ebri D, Chai RC, Corr AP, Smith JT, Morris JA, McDonald MM, Quinn JMW,
835 McGlade AR, Bartonicek N, Jansson M, Hatzikotoulas K et al. (2020) Osteocyte Transcriptome
836 Mapping Identifies a Molecular Landscape Controlling Skeletal Homeostasis and Susceptibility to
837 Skeletal Disease. *bioRxiv*: 2020.04.20.051409
838 Zeltz C, Gullberg D (2016) The integrin–collagen connection – a glue for tissue repair? *Journal of Cell*
839 *Science* 129: 653
840 Zhao A, Qin H, Fu X (2016) What Determines the Regenerative Capacity in Animals? *BioScience* 66:
841 735-746

842